

# Department of Electrical and Computer Engineering

Gainesville, Florida 32611



UNIVERSITY OF  
FLORIDA

**20071116225**

**MIMO Radar**  
**- Diversity Means Superiority**

**Jian Li**

Department of Electrical and Computer Engineering  
P.O.Box 116130

University of Florida, Gainesville, FL 32611

Phone: (352) 392-2642; Fax: (352) 392-0044; Email: li@dsp.ufl.edu

Annual report for the Office of Naval Research

Grant No. N00014-07-1-0293

November 2006 - October 2007

**Best Available Copy**

REPORT DOCUMENTATION PAGE				Form Approved OMB No. 0704-0188	
<p>The public reporting burden for this collection of information is estimated to average 1 hour per response, including the time for reviewing instructions, searching existing data sources, gathering and maintaining the data needed, and completing and reviewing the collection of information. Send comments regarding this burden estimate or any other aspect of this collection of information, including suggestions for reducing the burden, to Department of Defense, Washington Headquarters Services, Directorate for Information Operations and Reports (0704-0188), 1215 Jefferson Davis Highway, Suite 1204, Arlington, VA 22202-4302. Respondents should be aware that notwithstanding any other provision of law, no person shall be subject to any penalty for failing to comply with a collection of information if it does not display a currently valid OMB control number.</p> <p><b>PLEASE DO NOT RETURN YOUR FORM TO THE ABOVE ADDRESS.</b></p>					
1. REPORT DATE (DD-MM-YYYY) 25-10-2007		2. REPORT TYPE Annual Report		3. DATES COVERED (From - To) Nov. 2006 - Oct. 2007	
4. TITLE AND SUBTITLE Multi-Input Multi-Output (MIMO) Radar - Diversity Means Superiority			5a. CONTRACT NUMBER N00014-07-1-0293		
			5b. GRANT NUMBER N00014-07-1-0293		
			5c. PROGRAM ELEMENT NUMBER		
6. AUTHOR(S)  Li, Jian			5d. PROJECT NUMBER 00064512		
			5e. TASK NUMBER		
			5f. WORK UNIT NUMBER		
7. PERFORMING ORGANIZATION NAME(S) AND ADDRESS(ES) Department of Electrical and Computer Engineering P. O. Box 116130, University of Florida Gainesville, FL 32611				8. PERFORMING ORGANIZATION REPORT NUMBER N/A	
9. SPONSORING/MONITORING AGENCY NAME(S) AND ADDRESS(ES) Office of Naval Research 875 North Randolph Street Arlington, VA 22203-1995				10. SPONSOR/MONITOR'S ACRONYM(S) ONR	
				11. SPONSOR/MONITOR'S REPORT NUMBER(S) N/A	
12. DISTRIBUTION/AVAILABILITY STATEMENT  Approved for public release; distribution unlimited					
13. SUPPLEMENTARY NOTES None					
14. ABSTRACT  We consider a multiple-input multiple-output (MIMO) radar system where both the transmitter and receiver have multiple well-separated subarrays with each subarray containing closely-spaced antennas. Because of this general antenna configuration, both the coherent processing gain and the spatial diversity gain can be simultaneously achieved. We compare several spatial spectral estimators, including Capon and APES, for target detection and parameter estimation. We introduce a generalized likelihood ratio test (GLRT) and a conditional generalized likelihood ratio test (cGLRT) for the general antenna configuration. Based on GLRT and cGLRT, we then propose an iterative GLRT (iGLRT) procedure for target detection and parameter estimation. Via several numerical examples, we show that iGLRT can provide excellent detection and estimation performance at a low computational cost.					
15. SUBJECT TERMS Adaptive arrays, MIMO Radar, detection, localization, parameter estimation, growth-curve (GC) model, block-diagonal growth-curve (BDGC) model, generalized likelihood ratio test (GLRT).					
16. SECURITY CLASSIFICATION OF:			17. LIMITATION OF ABSTRACT	18. NUMBER OF PAGES	19a. NAME OF RESPONSIBLE PERSON
a. REPORT	b. ABSTRACT	c. THIS PAGE			Jian Li
U	U	U	U	39	19b. TELEPHONE NUMBER (Include area code) (352) 392-2642

## TABLE OF CONTENTS

	<u>page</u>
LIST OF FIGURES . . . . .	iii
ABSTRACT . . . . .	iv
CHAPTER	
1 INTRODUCTION . . . . .	1
2 SIGNAL MODEL . . . . .	4
3 SPATIAL SPECTRAL ESTIMATORS . . . . .	6
3.1 Capon . . . . .	6
3.2 APES . . . . .	7
4 GENERALIZED LIKELIHOOD RATIO TEST . . . . .	9
4.1 Generalized Likelihood Ratio Test (GLRT) . . . . .	9
4.2 Conditional Generalized Likelihood Ratio Test (cGLRT) . . . . .	12
4.3 Iterative Generalized Likelihood Ratio Test (iGLRT) . . . . .	18
5 NUMERICAL EXAMPLES . . . . .	20
5.1 Cramér-Rao bound . . . . .	20
5.2 Target Detection and Localization . . . . .	22
6 CONCLUSIONS . . . . .	29
A CRAMÉR-RAO BOUND . . . . .	30
REFERENCES . . . . .	33

**Best Available Copy**

## LIST OF FIGURES

<u>Figure</u>	<u>page</u>
5-1 Cumulative density functions of the Cramér-Rao bounds for (a) $\theta_1$ and (b) $\theta_3$ . . . . .	21
5-2 Outage CRB versus SNR. (a) $\text{CRB}_{0,01}$ for $\theta_1$ , (b) $\text{CRB}_{0,01}$ for $\theta_2$ , (c) $\text{CRB}_{0,1}$ for $\theta_1$ , and (d) $\text{CRB}_{0,1}$ for $\theta_2$ . . . . .	24
5-3 Spatial spectra, and GLR and cGLR Pseudo-Spectra, when $\theta_1 = -40^\circ$ , $\theta_2 = -20^\circ$ , and $\theta_3 = 0^\circ$ . (a) LS, (b) Capon, (c) APES, (d) GLRT, and (e) iGLRT. . . . .	25
5-4 Spatial spectra, and GLR and cGLR Pseudo-Spectra, when $\theta_1 = -40^\circ$ , $\theta_2 = -4^\circ$ , and $\theta_3 = 0^\circ$ . (a) Capon, (b) APES, (c) GLRT, and (d) iGLRT. . . . .	26
5-5 GLR and cGLR Pseudo-Spectra obtained in Steps I and II of iGLRT, when $\theta_1 = -40^\circ$ , $\theta_2 = -4^\circ$ , and $\theta_3 = 0^\circ$ . (a) $\rho(\theta)$ , (b) $\rho(\theta \hat{\theta}_1)$ , (c) $\rho(\theta \hat{\theta}_1, \hat{\theta}_2)$ , and (d) $\rho(\theta \hat{\theta}_1, \hat{\theta}_2, \hat{\theta}_3)$ . . . . .	27
5-6 Cumulative density functions of the CRBs and MSEs for (a) $\theta_1$ and (b) $\theta_3$ . . . . .	27
5-7 Outage $\text{CRB}_{0,1}$ and $\text{MSE}_{0,1}$ versus SNR for (a) $\theta_1$ and (b) $\theta_3$ . . . . .	28
5-8 Outage $\text{CRB}_{0,1}$ and $\text{MSE}_{0,1}$ versus number of data samples for (a) $\theta_1$ and (b) $\theta_3$ . . . . .	28



## Abstract

We consider a multiple-input multiple-output (MIMO) radar system where both the transmitter and receiver have multiple well-separated subarrays with each subarray containing closely-spaced antennas. Because of this general antenna configuration, both the coherent processing gain and the spatial diversity gain can be simultaneously achieved. We compare several spatial spectral estimators, including Capon and APES, for target detection and parameter estimation. We introduce a generalized likelihood ratio test (GLRT) and a conditional generalized likelihood ratio test (cGLRT) for the general antenna configuration. Based on GLRT and cGLRT, we then propose an iterative GLRT (iGLRT) procedure for target detection and parameter estimation. Via several numerical examples, we show that iGLRT can provide excellent detection and estimation performance at a low computational cost.

## CHAPTER 1 INTRODUCTION

A multiple-input multiple-output (MIMO) radar uses multiple antennas to simultaneously transmit several linearly independent waveforms. It also uses multiple antennas to receive the reflected signals. It has been shown that by exploiting this waveform diversity, MIMO radar can overcome performance degradations caused the radar cross-section (RCS) fluctuations [1] - [4], achieve flexible spatial transmit beam-pattern design [5] [6], provide high-resolution spatial spectral estimates [7] - [17], and significantly improve the parameter identifiability [18].

The statistical MIMO radar, studied in [1] - [4], aims at resisting the “scintillation” effect encountered in radar systems. It is well-known that the RCS of a target, which represents the amount of energy reflected from the target toward the receiver, changes rapidly as a function of the target aspect [19], and the locations of the transmitting and receiving antennas. The target scintillation causes severe degradations in the target detection and estimation performance of the radar. By spacing the transmit antennas, which transmit linearly independent signals, far away from each other, a spatial diversity gain can be obtained as in the MIMO wireless communications to this scintillation effect [1] - [4].

Flexible transmit beampattern designs are investigated in [5] [6]. Different from the statistical MIMO radar, the transmitting antennas are closely spaced. The authors in [5] and [6] show that the waveforms transmitted via closely spaced antennas can be optimized to obtain several transmit beampattern designs with superior performance. For example, the covariance matrix of the waveforms can be optimized to maximize the power around the locations of interest and also to minimize the cross-correlation of the signals reflected back to the radar by these targets, thereby

significantly improving the performance of the adaptive MIMO radar techniques. Due to the significantly larger number of degrees-of-freedom of a MIMO system, improved transmit beampatterns can be achieved with a MIMO radar than with its phased-array counterpart.

In [9], a MIMO radar technique is suggested to improve the radar resolution. The idea is to transmit  $N$  ( $N > 1$ ) orthogonal coded waveforms by  $N$  antennas and to receive the reflected signals by  $M$  ( $M > 1$ ) antennas. At each receiving antenna output, the signal is matched-filtered using each of the transmitted waveforms to obtain  $NM$  channels, where the data-adaptive Capon beamformer [20] is applied. It is proved in [9] that the beampattern of the proposed MIMO radar is obtained by the multiplication of the transmitting and receiving beampatterns, hence it has high resolution. However, [9] considers only single-target scenarios.

A MIMO radar scheme is considered in [16] and [17] that can deal with the presence of multiple targets. Similar to some of the MIMO radar approaches [5] - [15], linearly independent waveforms are transmitted simultaneously via multiple antennas. Due to the different phase shifts associated with different propagation paths from transmitting antennas to targets, these independent waveforms are linearly combined at the targets with different phase factors. As a result, the signal waveforms reflected from different targets are linearly independent, allowing the direct application of many adaptive techniques to achieve higher resolution and interference rejection capability. Several adaptive nonparametric algorithms, some of which also model steering vector errors, are presented in [16] and [17].

The MIMO radars discussed above can be grouped into two classes according to their antenna configurations. One class is the conventional radar array, in which both the transmitting and receiving antennas are closely spaced for coherent transmission and detection [5] - [17]. The class other is the diverse antenna configuration, where the antennas are separated far away from each other to achieve spatial diversity gain



[1] - [4]. To exploit the benefits of both schemes, we consider a general antenna configuration in this report, i.e., both the transmitting and receiving antenna arrays consist of several well-separated subarrays with each subarray containing closely-spaced antennas. We establish the growth curve models [21] - [24] and devise several estimators for the proposed MIMO radar system.

The remainder of this report is organized as follows. Chapter 2 presents the MIMO radar signal model. In Chapter 3, we discuss two adaptive spatial spectral estimators including Capon [20] and APES [25]. In Chapter 4, we introduce a generalized likelihood ratio test (GLRT) and a conditional generalized likelihood ratio test (cGLRT), and then propose an iterative GLRT (iGLRT) procedure for target detection and parameter estimation. Numerical examples are provided in Chapter 5.

## CHAPTER 2 SIGNAL MODEL

Consider a narrow-band MIMO radar system with  $\tilde{N}$  and  $\tilde{M}$  subarrays for transmitting and receiving, respectively. The  $n$ th transmit and  $m$ th receive subarrays have, respectively,  $N_n$  and  $M_m$  closely-spaced antennas,  $n = 1, 2, \dots, \tilde{N}$ , and  $m = 1, 2, \dots, \tilde{M}$ . We assume that the subarrays are sufficiently separated, and hence, for each target, its radar cross-sections (RCS) for different transmit and receive subarray pairs are statistically independent of each other. Let  $\mathbf{v}_n(\theta)$  and  $\mathbf{a}_m(\theta)$  be the steering vectors of the  $n$ th transmitting subarray and the  $m$ th receiving subarray, respectively, where  $\theta$  denotes the target location parameter, for example its angular location. Let the rows of  $\Phi_n$  be the waveforms transmitted from the antennas of the  $n$ th transmit subarray. We assume that the arrival time is known. Then, the signal received by the  $m$ th subarray due to the reflection of the target at  $\theta$  can be written as

$$\mathbf{X}_m = \sum_{n=1}^{\tilde{N}} \mathbf{a}_m(\theta) \beta_{mn,\theta} \mathbf{v}_n^T(\theta) \Phi_n + \mathbf{Z}_m, \quad m = 1, \dots, \tilde{M} \quad (2-1)$$

where  $\beta_{mn,\theta}$  is the complex amplitude proportional to the RCS for the  $(m, n)$ th receive and transmit subarray pair and for the target at the location  $\theta$ . The matrix  $\mathbf{Z}_m$  denotes a residual term for the unmodelled noise, e.g., interferences from targets other than  $\theta$  and at other range bins, and intentional or unintentional jamming. For notational simplicity, we will not show explicitly the dependence of  $\mathbf{Z}_m$  on  $\theta$ .

Let

$$\mathbf{X} = [\mathbf{X}_1^T \cdots \mathbf{X}_{\tilde{M}}^T]^T \in \mathbb{C}^{M \times L}, \quad (2-2)$$

$$\mathbf{A}(\theta) = \text{Diag}[\mathbf{a}_1(\theta), \dots, \mathbf{a}_{\tilde{M}}(\theta)] \in \mathbb{C}^{M \times \tilde{M}}, \quad (2-3)$$

$$\mathbf{V}(\theta) = \text{Diag}[\mathbf{v}_1(\theta), \dots, \mathbf{v}_{\tilde{N}}(\theta)] \in \mathbb{C}^{N \times \tilde{N}}, \quad (2-4)$$

and

$$\mathbf{\Phi} = [\mathbf{\Phi}_1^T \cdots \mathbf{\Phi}_{\tilde{N}}^T]^T \in \mathbb{C}^{N \times L}, \quad (2-5)$$

where  $M = M_1 + \cdots + M_{\tilde{M}}$  and  $N = N_1 + \cdots + N_{\tilde{N}}$  are the total numbers of receive and transmit antennas, respectively,  $L$  is the number of data samples of the transmitted waveforms,  $(\cdot)^T$  denotes the transpose operator, and  $\text{Diag}(\mathbf{a}_1, \cdots, \mathbf{a}_{\tilde{M}})$  is a block-diagonal matrix with  $\mathbf{a}_1, \cdots, \mathbf{a}_{\tilde{M}}$  being its diagonal submatrices. Then, (2-4) can be rewritten in the growth-curve (GC) model [21] - [22]:

$$\mathbf{X} = \mathbf{A}(\theta)\mathbf{B}_\theta\mathbf{S}(\theta) + \mathbf{Z}, \quad (2-6)$$

where the  $(m, n)$ th element of the  $\tilde{M} \times \tilde{N}$  matrix  $\mathbf{B}_\theta$  is  $\beta_{mn, \theta}$ ,  $\mathbf{Z}$  is defined similarly to  $\mathbf{X}$  in (2-2), and the rows of  $\mathbf{S}(\theta)$  are the reflected waveforms by the target at location  $\theta$ , i.e.,

$$\mathbf{S}(\theta) = \mathbf{V}^T(\theta)\mathbf{\Phi}. \quad (2-7)$$

Note that when  $\tilde{N} = \tilde{M} = 1$ , the signal model in (2-6) reduces to the MIMO radar model in [16] - [17], whereas when  $N = \tilde{N}$  and  $M = \tilde{M}$  it reduces to the diversity data model in [1] - [3]. Based on this data model. We below derive two classes of nonparametric methods, i.e., spatial spectral estimation and generalized likelihood ratio test (GLRT), for target detection and localization.

## CHAPTER 3

### SPATIAL SPECTRAL ESTIMATORS

We discuss two spatial spectral estimators for the proposed MIMO radar system. We use these methods to estimate the complex amplitudes in  $\mathbf{B}_\theta$  for each  $\theta$  of interest from the observed data matrix  $\mathbf{X}$ . The Frobenius norm of the estimated  $\hat{\mathbf{B}}_\theta$  forms a spatial spectrum in the 1D case or a radar image in the 2D case. We can then estimate the number of targets and their locations by searching for the peaks in the estimated spectrum (or image).

A simple way to estimate  $\mathbf{B}_\theta$  in (2-6) is via the Least-Squares (LS) method:

$$\hat{\mathbf{B}}_{\text{LS},\theta} = [\mathbf{A}^H(\theta)\mathbf{A}(\theta)]^{-1}\mathbf{A}(\theta)\mathbf{X}\mathbf{S}^H(\theta)[\mathbf{S}(\theta)\mathbf{S}^H(\theta)]^{-1}, \quad (3-1)$$

where  $(\cdot)^H$  denotes the conjugate transpose. However, as any other data-independent beamforming-type method, the LS method suffers from high-sidelobes and low resolution. In the presence of strong interference and jamming, the method completely fails to work. Hence, we discuss two robust adaptive spatial spectral estimation approaches that offer higher resolution and interference suppression capabilities.

### 3.1 Capon

The Capon estimator for  $\mathbf{B}_\theta$  in (2-6) consists of two main steps [20], [26], [22]. The first step is a generalized Capon beamforming step. The second step is an LS estimation step, which involves a matched filter to the known waveform  $\mathbf{S}(\theta)$ .

The generalized Capon beamformer can be formulated as follows:

$$\min_{\mathbf{W}} \text{tr}(\mathbf{W}^H\mathbf{R}\mathbf{W}) \quad \text{subject to} \quad \mathbf{W}^H\mathbf{A}(\theta) = \mathbf{I}, \quad (3-2)$$

where  $\mathbf{W} \in \mathbb{C}^{M \times \tilde{M}}$  is the weighting matrix used to achieve noise, interference and jamming suppression while keeping the desired signal undistorted,  $\text{tr}(\cdot)$  denotes the



trace of a matrix, and

$$\hat{\mathbf{R}} = \frac{1}{L} \mathbf{X} \mathbf{X}^H \quad (3-3)$$

is the sample covariance matrix with  $L$  being the number of data samples.

Solving the optimization problem in (3-2), we have:

$$\hat{\mathbf{W}}_{\text{Capon}} = \hat{\mathbf{R}}^{-1} \mathbf{A}(\theta) [\mathbf{A}^H(\theta) \hat{\mathbf{R}}^{-1} \mathbf{A}(\theta)]^{-1}. \quad (3-4)$$

By using (2-6) and (3-4), the output of the Capon beamformer can be written as

$$[\mathbf{A}^H(\theta) \hat{\mathbf{R}}^{-1} \mathbf{A}(\theta)]^{-1} \mathbf{A}^H(\theta) \hat{\mathbf{R}}^{-1} \mathbf{X} = \mathbf{B}_\theta \mathbf{S}(\theta) + [\mathbf{A}^H(\theta) \hat{\mathbf{R}}^{-1} \mathbf{A}(\theta)]^{-1} \mathbf{A}^H(\theta) \hat{\mathbf{R}}^{-1} \mathbf{Z}. \quad (3-5)$$

By applying the least-squares (LS) method to (3-5), the Capon estimate of  $\mathbf{B}_\theta$  follows:

$$\hat{\mathbf{B}}_{\text{Capon},\theta} = [\mathbf{A}^H(\theta) \hat{\mathbf{R}}^{-1} \mathbf{A}(\theta)]^{-1} \mathbf{A}^H(\theta) \hat{\mathbf{R}}^{-1} \mathbf{X} \mathbf{S}^H(\theta) [\mathbf{S}(\theta) \mathbf{S}^H(\theta)]^{-1}. \quad (3-6)$$

### 3.2 APES

The generalized APES method is a straightforward extension of the APES method [25] [27], which can be formulated as:

$$\min_{\mathbf{W}, \mathbf{B}} \|\mathbf{W}^H \mathbf{X} - \mathbf{B}_\theta \mathbf{S}(\theta)\|^2 \quad \text{subject to} \quad \mathbf{W}^H \mathbf{A}(\theta) = \mathbf{I}. \quad (3-7)$$

where  $\|\cdot\|$  denotes the Frobenius norm, and  $\mathbf{W}$  is the weighting matrix. Minimizing the cost function in (3-7) with respect to  $\mathbf{B}_\theta$  yields:

$$\hat{\mathbf{B}}_{\text{APES},\theta} = \mathbf{W}^H \mathbf{X} \mathbf{S}^H(\theta) [\mathbf{S}(\theta) \mathbf{S}^H(\theta)]^{-1}. \quad (3-8)$$

Then, the optimization problem reduces to

$$\min \text{tr}(\mathbf{W}^H \hat{\mathbf{Q}} \mathbf{W}) \quad \text{subject to} \quad \mathbf{W}^H \mathbf{A}(\theta) = \mathbf{I}, \quad (3-9)$$

with

$$\hat{\mathbf{Q}} = \hat{\mathbf{R}} - \frac{1}{L} \mathbf{X} \mathbf{S}^H(\theta) [\mathbf{S}(\theta) \mathbf{S}^H(\theta)]^{-1} \mathbf{S}(\theta) \mathbf{X}^H. \quad (3-10)$$

For notional simplicity, we have omitted the dependence of  $\hat{\mathbf{Q}}$  on  $\theta$ .

Solving the optimization problem of (3-9) gives the generalized APES beamformer weighting matrix:

$$\hat{\mathbf{W}}_{\text{APES},\theta} = \hat{\mathbf{Q}}^{-1} \mathbf{A}(\theta) [\mathbf{A}^H(\theta) \hat{\mathbf{Q}} \mathbf{A}(\theta)]^{-1}. \quad (3-11)$$

Inserting (3-11) in (3-8), we readily get the APES estimate of  $\mathbf{B}_\theta$  as:

$$\hat{\mathbf{B}}_{\text{APES},\theta} = [\mathbf{A}^H(\theta) \hat{\mathbf{Q}}^{-1} \mathbf{A}(\theta)]^{-1} \mathbf{A}^H(\theta) \hat{\mathbf{Q}}^{-1} \mathbf{X} \mathbf{S}^H(\theta) [\mathbf{S}(\theta) \mathbf{S}^H(\theta)]^{-1}. \quad (3-12)$$

Interestingly, we note that (3-12) has the same form as the ML estimate in [21] and [22]. However, the APES estimate is derived based on the beamforming method, and, unlike the ML in [21] and [22], it does not need probability density function (pdf) of  $\mathbf{Z}$ .

## CHAPTER 4

### GENERALIZED LIKELIHOOD RATIO TEST

Generalized likelihood ratio test (GLRT) has been used widely for target detection and localization. We derive below a GLRT and a conditional generalized likelihood ratio test (cGLRT) for the proposed MIMO radar, and then propose an iterative GLRT (iGLRT) procedure for improved performance.

#### 4.1 Generalized Likelihood Ratio Test (GLRT)

Throughout this chapter, we assume that the columns of the interference and noise term  $\mathbf{Z}$  in (2-6) are independently and identically distributed (*i.i.d.*) circularly symmetric complex Gaussian random vectors with mean zero and an unknown covariance matrix  $\mathbf{Q}$ .

Consider the following hypothesis test problem:

$$\begin{cases} H_0 : & \mathbf{X} = \mathbf{Z} \\ H_1 : & \mathbf{X} = \mathbf{A}(\theta)\mathbf{B}_\theta\mathbf{S}(\theta) + \mathbf{Z}, \end{cases} \quad (4.1)$$

i.e., we want to test if there exists a target at location  $\theta$  or not. Similarly to [28] and [29], we define a generalized likelihood ratio (GLR) as follows:

$$\rho(\theta) = \left\{ 1 - \left[ \frac{\max_{\mathbf{Q}} f(\mathbf{X}|\mathbf{H}_0)}{\max_{\mathbf{B}_\theta, \mathbf{Q}} f(\mathbf{X}|\mathbf{H}_1)} \right]^{\frac{1}{L}} \right\}^L, \quad (4.2)$$

where  $f(\mathbf{X}|\mathbf{H}_i)$  ( $i = 0, 1$ ) is the pdf of  $\mathbf{X}$  under the hypothesis  $\mathbf{H}_i$ . From (4.2), we note that the value of the GLR,  $\rho(\theta)$ , lies between 0 and 1. If there is a target at a location  $\theta$  of interest, we have  $\max_{\mathbf{B}_\theta, \mathbf{Q}} f(\mathbf{X}|\mathbf{H}_1) \gg \max_{\mathbf{Q}} f(\mathbf{X}|\mathbf{H}_0)$ , i.e.,  $\rho \approx 1$ ; otherwise  $\rho \approx 0$ .

Under Hypothesis  $H_0$ , we have

$$f(\mathbf{X}|H_0) = \frac{1}{\pi^{LM}|\mathbf{Q}|^L} \exp\{-\text{tr}(\mathbf{Q}^{-1}\mathbf{X}\mathbf{X}^H)\}, \quad (4-3)$$

where  $|\cdot|$  denotes the determinant of a matrix. Maximizing (4-3) with respect to  $\mathbf{Q}$  yields:

$$\max_{\mathbf{Q}} f(\mathbf{X}|H_0) = (\pi e)^{-LM} |\hat{\mathbf{R}}|^{-L}, \quad (4-4)$$

where  $\hat{\mathbf{R}}$  is defined in (3-3).

Similarly, under Hypothesis  $H_1$ , we have

$$f(\mathbf{X}|H_1) = \frac{1}{\pi^{LM}|\mathbf{Q}|^L} \exp\left\{-\text{tr}\left\{\mathbf{Q}^{-1}[\mathbf{X} - \mathbf{A}(\theta)\mathbf{B}_\theta\mathbf{S}(\theta)][\mathbf{X} - \mathbf{A}(\theta)\mathbf{B}_\theta\mathbf{S}(\theta)]^H\right\}\right\}. \quad (4-5)$$

Maximizing (4-5) with respect to  $\mathbf{Q}$  yields:

$$\max_{\mathbf{Q}} f(\mathbf{X}|H_1) = (\pi e)^{-LM} \left| \frac{1}{L} [\mathbf{X} - \mathbf{A}(\theta)\mathbf{B}_\theta\mathbf{S}(\theta)][\mathbf{X} - \mathbf{A}(\theta)\mathbf{B}_\theta\mathbf{S}(\theta)]^H \right|^{-L}. \quad (4-6)$$

Hence, the optimization problem in the denominator of (4-2) reduces to

$$\min_{\mathbf{B}_\theta} \left| \frac{1}{L} [\mathbf{X} - \mathbf{A}(\theta)\mathbf{B}_\theta\mathbf{S}(\theta)][\mathbf{X} - \mathbf{A}(\theta)\mathbf{B}_\theta\mathbf{S}(\theta)]^H \right|. \quad (4-7)$$



Following [21] and [22] and dropping the dependence of  $\mathbf{A}$ ,  $\mathbf{S}$  and  $\mathbf{B}$  on  $\theta$  for notional convenience, we have:

$$\begin{aligned}
& \left| \frac{1}{L} [\mathbf{X} - \mathbf{A}\mathbf{B}\mathbf{S}] [\mathbf{X} - \mathbf{A}\mathbf{B}\mathbf{S}]^H \right| \\
&= \left| \frac{1}{L} [\mathbf{A}\mathbf{B} - \mathbf{X}\mathbf{S}^H(\mathbf{S}\mathbf{S}^H)^{-1}](\mathbf{S}\mathbf{S}^H)[\mathbf{A}\mathbf{B} - \mathbf{X}\mathbf{S}^H(\mathbf{S}\mathbf{S}^H)^{-1}]^H + \hat{\mathbf{Q}} \right| \\
&= |\hat{\mathbf{Q}}| \left| \mathbf{I} + \frac{1}{L} \hat{\mathbf{Q}}^{-\frac{1}{2}} [\mathbf{A}\mathbf{B} - \mathbf{X}\mathbf{S}^H(\mathbf{S}\mathbf{S}^H)^{-1}](\mathbf{S}\mathbf{S}^H)[\mathbf{A}\mathbf{B} - \mathbf{X}\mathbf{S}^H(\mathbf{S}\mathbf{S}^H)^{-1}]^H \hat{\mathbf{Q}}^{-\frac{1}{2}} \right| \\
&= |\hat{\mathbf{Q}}| \left| \mathbf{I} + \frac{1}{L} (\mathbf{S}\mathbf{S}^H)^{\frac{1}{2}} [\mathbf{A}\mathbf{B} - \mathbf{X}\mathbf{S}^H(\mathbf{S}\mathbf{S}^H)^{-1}]^H \hat{\mathbf{Q}}^{-1} \times \right. \\
&\quad \left. [\mathbf{A}\mathbf{B} - \mathbf{X}\mathbf{S}^H(\mathbf{S}\mathbf{S}^H)^{-1}](\mathbf{S}\mathbf{S}^H)^{\frac{1}{2}} \right| \tag{4-8} \\
&= |\hat{\mathbf{Q}}| \left| \mathbf{I} + \frac{1}{L} (\mathbf{S}\mathbf{S}^H)^{-\frac{1}{2}} \mathbf{S}\mathbf{X}^H [\hat{\mathbf{Q}}^{-1} - \hat{\mathbf{Q}}^{-1}\mathbf{A}(\mathbf{A}^H\hat{\mathbf{Q}}^{-1}\mathbf{A})^{-1}\mathbf{A}^H\hat{\mathbf{Q}}^{-1}] \mathbf{X}\mathbf{S}^H(\mathbf{S}\mathbf{S}^H)^{-\frac{1}{2}} \right. \\
&\quad \left. + \frac{1}{L} (\mathbf{S}\mathbf{S}^H)^{\frac{1}{2}} [\mathbf{B} - (\mathbf{A}^H\hat{\mathbf{Q}}^{-1}\mathbf{A})^{-1}\mathbf{A}^H\hat{\mathbf{Q}}^{-1}\mathbf{X}\mathbf{S}^H(\mathbf{S}\mathbf{S}^H)^{-1}]^H (\mathbf{A}^H\hat{\mathbf{Q}}^{-1}\mathbf{A}) \times \right. \\
&\quad \left. [\mathbf{B} - (\mathbf{A}^H\hat{\mathbf{Q}}^{-1}\mathbf{A})^{-1}\mathbf{A}^H\hat{\mathbf{Q}}^{-1}\mathbf{X}\mathbf{S}^H(\mathbf{S}\mathbf{S}^H)^{-1}](\mathbf{S}\mathbf{S}^H)^{\frac{1}{2}} \right| \\
&\geq |\hat{\mathbf{Q}}| \left| \mathbf{I} + \frac{1}{L} (\mathbf{S}\mathbf{S}^H)^{-\frac{1}{2}} \mathbf{S}\mathbf{X}^H [\hat{\mathbf{Q}}^{-1} - \hat{\mathbf{Q}}^{-1}\mathbf{A}(\mathbf{A}^H\hat{\mathbf{Q}}^{-1}\mathbf{A})^{-1}\mathbf{A}^H\hat{\mathbf{Q}}^{-1}] \mathbf{X}\mathbf{S}^H(\mathbf{S}\mathbf{S}^H)^{-\frac{1}{2}} \right| \tag{4-9}
\end{aligned}$$

where  $\hat{\mathbf{Q}}$  is defined in (3-10). To get (4-8), we have used the fact that  $|\mathbf{I} + \mathbf{X}\mathbf{Y}| = |\mathbf{I} + \mathbf{Y}\mathbf{X}|$  [30], and the equality in (4-9) holds when  $\mathbf{B}$  equates to the APES estimate in (3-12). Note that

$$\begin{aligned}
& |\hat{\mathbf{Q}}| \left| \mathbf{I} + \frac{1}{L} (\mathbf{S}\mathbf{S}^H)^{-\frac{1}{2}} \mathbf{S}\mathbf{X}^H [\hat{\mathbf{Q}}^{-1} - \hat{\mathbf{Q}}^{-1}\mathbf{A}(\mathbf{A}^H\hat{\mathbf{Q}}^{-1}\mathbf{A})^{-1}\mathbf{A}^H\hat{\mathbf{Q}}^{-1}] \mathbf{X}\mathbf{S}^H(\mathbf{S}\mathbf{S}^H)^{-\frac{1}{2}} \right| \\
&= |\hat{\mathbf{Q}}| |\mathbf{I} + [\hat{\mathbf{Q}}^{-1} - \hat{\mathbf{Q}}^{-1}\mathbf{A}(\mathbf{A}^H\hat{\mathbf{Q}}^{-1}\mathbf{A})^{-1}\mathbf{A}^H\hat{\mathbf{Q}}^{-1}](\hat{\mathbf{R}} - \hat{\mathbf{Q}})| \\
&= |\hat{\mathbf{R}} - \mathbf{A}(\mathbf{A}^H\hat{\mathbf{Q}}^{-1}\mathbf{A})^{-1}\mathbf{A}^H\hat{\mathbf{Q}}^{-1}(\hat{\mathbf{R}} - \hat{\mathbf{Q}})| \\
&= |\hat{\mathbf{R}}| |\mathbf{I} - \mathbf{A}^H(\mathbf{A}^H\hat{\mathbf{Q}}^{-1}\mathbf{A})^{-1}\mathbf{A}^H(\hat{\mathbf{Q}}^{-1} - \hat{\mathbf{R}}^{-1})| \\
&= |\hat{\mathbf{R}}| |(\mathbf{A}^H\hat{\mathbf{Q}}^{-1}\mathbf{A})^{-1}(\mathbf{A}^H\hat{\mathbf{R}}^{-1}\mathbf{A})|, \tag{4-10}
\end{aligned}$$

From (4-6), (4-9) and (4-10), it follows that

$$\max_{\mathbf{B}_\theta, \mathbf{Q}} f(\mathbf{X}|\mathbf{H}_1) = (\pi e)^{-LM} |\hat{\mathbf{R}}|^{-L} |\mathbf{A}^H(\theta)\hat{\mathbf{Q}}^{-1}\mathbf{A}(\theta)|^L |\mathbf{A}^H(\theta)\hat{\mathbf{R}}^{-1}\mathbf{A}(\theta)|^{-L}. \tag{4-11}$$

Substituting (4-4) and (4-11) into (4-2) yields:

$$\rho(\theta) = \left\{ 1 - \frac{|\mathbf{A}^H(\theta)\hat{\mathbf{R}}^{-1}\mathbf{A}(\theta)|}{|\mathbf{A}^H(\theta)\hat{\mathbf{Q}}^{-1}\mathbf{A}(\theta)|} \right\}^L. \quad (4-12)$$

We remark that when there are multiple targets, and the number of targets (say  $K$ ) are known *a priori*, the GLRT in (4-12) can be extended to a multivariate counterpart by considering the following hypothesis testing problem:

$$\begin{cases} H_0 : & \mathbf{X} = \mathbf{Z} \\ H_K : & \mathbf{X} = \sum_{k=1}^K \mathbf{A}(\theta_k)\mathbf{B}_{\theta_k}\mathbf{S}(\theta_k) + \mathbf{Z}. \end{cases} \quad (4-13)$$

As a parametric method, this multivariate GLRT can provide better target detection and parameter estimation performance than its univariate counterpart. However, the multivariate GLRT is computationally intensive because it needs to search in the  $K$ -dimensional parameter space  $\{\theta_k\}_{k=1}^K$ . Moreover, the number of targets is hardly known *a priori* in practice.

We propose below an iterative GLRT (iGLRT), which require only one-dimensional search (like the univariate GLRT), but provides a target detection and parameter estimation performance close to the multivariate GLRT.

## 4.2 Conditional Generalized Likelihood Ratio Test (cGLRT)

Before we describe the iGLRT procedure, we first consider the following hypothesis testing problem, referred to as the conditional generalized likelihood ratio test (cGLRT). Suppose that we know that there are  $p$  targets at the locations  $\{\hat{\theta}_k\}_{k=1}^p$ , and we want to determine if there are any additional targets. This problem can be formulated in the following hypothesis testing problem:

$$\begin{cases} H_p : & \mathbf{X} = \sum_{k=1}^p \mathbf{A}(\hat{\theta}_k)\mathbf{B}_{\hat{\theta}_k}\mathbf{S}(\hat{\theta}_k) + \mathbf{Z} \\ H_{p+1} : & \mathbf{X} = \mathbf{A}(\theta)\mathbf{B}_\theta\mathbf{S}(\theta) + \sum_{k=1}^p \mathbf{A}(\hat{\theta}_k)\mathbf{B}_{\hat{\theta}_k}\mathbf{S}(\hat{\theta}_k) + \mathbf{Z}. \end{cases} \quad (4-14)$$

Note that both the equations in (4-14) are in the form of the block-diagonal growth curve (BDGC) model studied in [24]. For convenience, we rewrite (4-14) as:

$$\begin{cases} H_p : & \mathbf{X} = \tilde{\mathbf{A}}_p \tilde{\mathbf{B}}_p \tilde{\mathbf{S}}_p + \mathbf{Z} \\ H_{p+1} : & \mathbf{X} = \tilde{\mathbf{A}}_{p+1} \tilde{\mathbf{B}}_{p+1} \tilde{\mathbf{S}}_{p+1} + \mathbf{Z}, \end{cases} \quad (4-15)$$

where

$$\tilde{\mathbf{B}}_p = \text{Diag}(\mathbf{B}_{\hat{\theta}_1}, \dots, \mathbf{B}_{\hat{\theta}_p}) \quad (4-16)$$

$$\tilde{\mathbf{A}}_p = [\mathbf{A}(\hat{\theta}_1) \dots \mathbf{A}(\hat{\theta}_p)], \quad (4-17)$$

$$\tilde{\mathbf{S}}_p = [\mathbf{S}^T(\hat{\theta}_1) \dots \mathbf{S}^T(\hat{\theta}_p)]^T, \quad (4-18)$$

$$\tilde{\mathbf{B}}_{p+1} = \text{Diag}(\mathbf{B}_\theta, \mathbf{B}_{\hat{\theta}_1}, \dots, \mathbf{B}_{\hat{\theta}_p}) \quad (4-19)$$

$$\tilde{\mathbf{A}}_{p+1} = [\mathbf{A}(\theta) \mathbf{A}(\hat{\theta}_1) \dots \mathbf{A}(\hat{\theta}_p)], \quad (4-20)$$

$$\tilde{\mathbf{S}}_{p+1} = [\mathbf{S}^T(\theta) \mathbf{S}^T(\hat{\theta}_1) \dots \mathbf{S}^T(\hat{\theta}_p)]^T. \quad (4-21)$$

Similarly, we define a conditional generalized likelihood ratio (cGLR) as follows:

$$\rho(\theta | \{\hat{\theta}_k\}_{k=1}^p) = \left\{ 1 - \left[ \frac{\max_{\tilde{\mathbf{B}}_p, \mathbf{Q}} f(\mathbf{X} | H_p)}{\max_{\tilde{\mathbf{B}}_{p+1}, \mathbf{Q}} f(\mathbf{X} | H_{p+1})} \right]^{\frac{1}{L}} \right\}^L, \quad (4-22)$$

where  $f(\mathbf{X} | H_i)$  is the pdf of  $\mathbf{X}$  under the  $H_i$  hypothesis, and  $\mathbf{Q}$  is the covariance matrix of the columns of  $\mathbf{Z}$ .

We first consider the optimization problem of the numerator in (4-22). Maximizing  $f(\mathbf{X} | H_p)$  with respect to  $\mathbf{Q}$  yields:

$$\max_{\mathbf{Q}} f(\mathbf{X} | H_p) = (\pi e)^{-ML} \left| \frac{1}{L} (\mathbf{X} - \tilde{\mathbf{A}}_p \tilde{\mathbf{B}}_p \tilde{\mathbf{S}}_p) (\mathbf{X} - \tilde{\mathbf{A}}_p \tilde{\mathbf{B}}_p \tilde{\mathbf{S}}_p)^H \right|^{-L}. \quad (4-23)$$

Hence, the optimization problem reduces to

$$\min_{\tilde{\mathbf{B}}_p} \left| \frac{1}{L} (\mathbf{X} - \tilde{\mathbf{A}}_p \tilde{\mathbf{B}}_p \tilde{\mathbf{S}}_p) (\mathbf{X} - \tilde{\mathbf{A}}_p \tilde{\mathbf{B}}_p \tilde{\mathbf{S}}_p)^H \right| \quad \text{with} \quad \tilde{\mathbf{B}}_p = \text{Diag}(\mathbf{B}_{\hat{\theta}_1}, \dots, \mathbf{B}_{\hat{\theta}_p}). \quad (4-24)$$

The optimization problem in (4-24) does not appear to admit a closed-form solution because  $\tilde{\mathbf{B}}_p$  is a block-diagonal matrix. Herein, we adopt a technique used in [31] to approximate a closed-form solution.

Note that

$$\begin{aligned}
& \left| \frac{1}{L} (\mathbf{X} - \tilde{\mathbf{A}}_p \tilde{\mathbf{B}}_p \tilde{\mathbf{S}}_p) (\mathbf{X} - \tilde{\mathbf{A}}_p \tilde{\mathbf{B}}_p \tilde{\mathbf{S}}_p)^H \right| \\
&= \left| \frac{1}{L} (\mathbf{X} - \tilde{\mathbf{A}}_p \tilde{\mathbf{B}}_p \tilde{\mathbf{S}}_p) (\Pi_{\tilde{\mathbf{S}}_p} + \Pi_{\tilde{\mathbf{S}}_p}^\perp) (\mathbf{X} - \tilde{\mathbf{A}}_p \tilde{\mathbf{B}}_p \tilde{\mathbf{S}}_p)^H \right| \\
&= \left| \frac{1}{L} (\mathbf{X} \Pi_{\tilde{\mathbf{S}}_p} - \tilde{\mathbf{A}}_p \tilde{\mathbf{B}}_p \tilde{\mathbf{S}}_p) (\mathbf{X} \Pi_{\tilde{\mathbf{S}}_p} - \tilde{\mathbf{A}}_p \tilde{\mathbf{B}}_p \tilde{\mathbf{S}}_p)^H + \tilde{\mathbf{Q}}_p \right| \\
&= \left| \frac{1}{L} (\mathbf{X} \Pi_{\tilde{\mathbf{S}}_p} - \tilde{\mathbf{A}}_p \tilde{\mathbf{B}}_p \tilde{\mathbf{S}}_p) (\mathbf{X} \Pi_{\tilde{\mathbf{S}}_p} - \tilde{\mathbf{A}}_p \tilde{\mathbf{B}}_p \tilde{\mathbf{S}}_p)^H \tilde{\mathbf{Q}}_p^{-1} + \mathbf{I} \right| |\tilde{\mathbf{Q}}_p|, \quad (4-25)
\end{aligned}$$

where

$$\Pi_{\tilde{\mathbf{S}}_p} = \tilde{\mathbf{S}}_p^H (\tilde{\mathbf{S}}_p \tilde{\mathbf{S}}_p^H)^- \tilde{\mathbf{S}}_p, \quad \Pi_{\tilde{\mathbf{S}}_p}^\perp = \mathbf{I} - \Pi_{\tilde{\mathbf{S}}_p}, \quad (4-26)$$

and

$$\tilde{\mathbf{Q}}_p = \frac{1}{L} \mathbf{X} \Pi_{\tilde{\mathbf{S}}_p}^\perp \mathbf{X}^H, \quad (4-27)$$

with  $(\cdot)^-$  denoting the generalized matrix inverse.

Consider the idempotent matrices  $\Pi_{\tilde{\mathbf{S}}_p}$  and  $\Pi_{\tilde{\mathbf{S}}_p}^\perp$ . Assume that the number of data samples is large enough, i.e.,  $L \gg \tilde{N}p$ . Note that  $\tilde{\mathbf{S}}_p$  is an  $\tilde{N}p \times L$  matrix. Hence, we have:

$$\text{rank}(\Pi_{\tilde{\mathbf{S}}_p}) \leq \tilde{N}p \quad \text{and} \quad \text{rank}(\Pi_{\tilde{\mathbf{S}}_p}^\perp) \geq L - \tilde{N}p, \quad (4-28)$$

with  $\text{rank}(\cdot)$  denoting the rank of a matrix. Then, we have

$$\tilde{\mathbf{Q}}_p = O(1), \quad (4-29)$$



and

$$\begin{aligned} & \frac{1}{L}(\mathbf{X}\Pi_{\tilde{\mathbf{S}}_p} - \tilde{\mathbf{A}}_p\tilde{\mathbf{B}}_p\tilde{\mathbf{S}}_p)(\mathbf{X}\Pi_{\tilde{\mathbf{S}}_p} - \tilde{\mathbf{A}}_p\tilde{\mathbf{B}}_p\tilde{\mathbf{S}}_p)^T \\ &= \frac{1}{L}(\mathbf{X} - \tilde{\mathbf{A}}_p\tilde{\mathbf{B}}_p\tilde{\mathbf{S}}_p)\Pi_{\tilde{\mathbf{S}}_p}(\mathbf{X} - \tilde{\mathbf{A}}_p\tilde{\mathbf{B}}_p\tilde{\mathbf{S}}_p)^T = O\left(\frac{1}{L}\right). \end{aligned} \quad (4-30)$$

Therefore, we get:

$$\frac{1}{L}(\mathbf{X}\Pi_{\tilde{\mathbf{S}}_p} - \tilde{\mathbf{A}}_p\tilde{\mathbf{B}}_p\tilde{\mathbf{S}}_p)(\mathbf{X}\Pi_{\tilde{\mathbf{S}}_p} - \tilde{\mathbf{A}}_p\tilde{\mathbf{B}}_p\tilde{\mathbf{S}}_p)^T \tilde{\mathbf{Q}}_p^{-1} = O\left(\frac{1}{L}\right) \ll 1. \quad (4-31)$$

Let  $\{\lambda_i\}_{i=1}^M$  be the eigenvalues of the matrix in (4-31), which satisfy that  $0 \leq \lambda_i \ll 1$ .

Through some matrix manipulations, we obtain:

$$\begin{aligned} & \left| \frac{1}{L}(\mathbf{X}\Pi_{\tilde{\mathbf{S}}_p} - \tilde{\mathbf{A}}_p\tilde{\mathbf{B}}_p\tilde{\mathbf{S}}_p)(\mathbf{X}\Pi_{\tilde{\mathbf{S}}_p} - \tilde{\mathbf{A}}_p\tilde{\mathbf{B}}_p\tilde{\mathbf{S}}_p)^T \tilde{\mathbf{Q}}_p^{-1} + \mathbf{I} \right| \\ &= \prod_{i=1}^M (1 + \lambda_i) \approx 1 + \sum_{i=1}^M \lambda_i \\ &= 1 + \frac{1}{L} \text{tr} \left[ (\mathbf{X}\Pi_{\tilde{\mathbf{S}}_p} - \frac{1}{L}\tilde{\mathbf{A}}_p\tilde{\mathbf{B}}_p\tilde{\mathbf{S}}_p)(\mathbf{X}\Pi_{\tilde{\mathbf{S}}_p} - \tilde{\mathbf{A}}_p\tilde{\mathbf{B}}_p\tilde{\mathbf{S}}_p)^T \tilde{\mathbf{Q}}_p^{-1} \right] \\ &= 1 + \frac{1}{L} \left\| \text{vec}(\tilde{\mathbf{Q}}_p^{-\frac{1}{2}} \mathbf{X}\Pi_{\tilde{\mathbf{S}}_p}) - \text{vec}(\tilde{\mathbf{Q}}_p^{-\frac{1}{2}} \tilde{\mathbf{A}}_p\tilde{\mathbf{B}}_p\tilde{\mathbf{S}}_p) \right\|^2, \end{aligned} \quad (4-32)$$

where  $\text{vec}(\cdot)$  denotes vectorization operator (stacking the columns of a matrix on top of each other), respectively, and  $\tilde{\mathbf{Q}}_p^{-\frac{1}{2}}$  is the Hermitian square root of  $\tilde{\mathbf{Q}}_p^{-1}$ . In (4-32), we have omitted the high-order terms of  $\{\lambda_i\}$  for the approximation.

Hence, for a large number of data samples, the optimization problem in (4-24) can be approximated as:

$$\begin{aligned} \min_{\tilde{\mathbf{B}}_p} \quad & \left\| \text{vec}(\tilde{\mathbf{Q}}_p^{-\frac{1}{2}} \mathbf{X}\Pi_{\tilde{\mathbf{S}}_p}) - \text{vec}(\tilde{\mathbf{Q}}_p^{-\frac{1}{2}} \tilde{\mathbf{A}}_p\tilde{\mathbf{B}}_p\tilde{\mathbf{S}}_p) \right\|^2. \\ \text{with } \tilde{\mathbf{B}}_p = & \text{Diag}(\mathbf{B}_{\hat{\theta}_1}, \dots, \mathbf{B}_{\hat{\theta}_p}). \end{aligned} \quad (4-33)$$

To solve the above optimization problem, we introduce below two partitioned matrix operations and two lemmas without proof (see [24] for the detailed proofs).

**Definition 1.** Let  $\mathbf{G}$  be a partitioned matrix with  $\mathbf{G}_{i,j}$  being the  $(i, j)$ th ( $i, j = 1, 2, \dots, J$ ) submatrix of  $\mathbf{G}$ . Then the block-diagonal vectorization operation is defined by

$$\text{vecb}(\mathbf{G}) \triangleq [\text{vec}(\mathbf{G}_{1,1})^T \text{vec}(\mathbf{G}_{2,2})^T \cdots \text{vec}(\mathbf{G}_{J,J})^T]^T. \quad (4-34)$$

**Definition 2.** Let  $\Sigma$  and  $\Omega$  be two partitioned matrices with conformal partitioning and with  $\Sigma_{i,j}$  and  $\Omega_{i,j}$  being the  $(i, j)$ th submatrices of  $\Sigma$  and  $\Omega$ , respectively. Then the generalized Khatri-Rao product [32] is defined by

$$[\Sigma \circledast \Omega]_{i,j} \triangleq \Sigma_{i,j} \otimes \Omega_{i,j}, \quad (4-35)$$

where  $[\cdot]_{i,j}$  denotes the  $(i, j)$ th submatrix of the given partitioned matrix and  $\otimes$  denotes the Kronecker matrix product.

Note that both the block-diagonal vectorization  $\text{vecb}(\cdot)$  and the generalized Khatri-Rao product  $\circledast$  are defined based on a particular matrix partitioning, i.e., different matrix partitionings will lead to different results. Throughout this report, the partitioned matrix operation are all based on the partitionings in (4-16) - (4-21). It is also worth pointing out that matrix partitioning may be “inherited” through matrix operations. For example, for the partitioned matrix  $\hat{\mathbf{A}}$  given by (4-18),  $\hat{\mathbf{A}}_p^H \hat{\mathbf{A}}_p$  is a  $p \times p$  partitioned matrix with the  $(i, j)$ th ( $i, j = 1, 2, \dots, p$ ) submatrix being  $\mathbf{A}^H(\hat{\theta}_i) \mathbf{A}(\hat{\theta}_j)$ .

**Lemma 1.** Let  $\Sigma$  and  $\Omega$  be two partitioned matrices with  $K$  block rows and  $J$  block columns, and let  $\mathbf{G}$  be a block-diagonal matrix with compatible dimensions and conformal partitioning with  $\Sigma$  and  $\Omega$ . Then

$$\text{vecb}(\Sigma \mathbf{G} \Omega^T) = (\Omega \circledast \Sigma) \text{vecb}(\mathbf{G}). \quad (4-36)$$

**Lemma 2.** Let  $\mathbf{U}$  and  $\mathbf{V}$  be two partitioned matrices with 1 block row and  $J$  block columns, and let  $\mathbf{H}$  and  $\mathbf{F}$  be two partitioned matrices with 1 block row and  $K$  block

columns and with compatible dimensions with  $\mathbf{U}$  and  $\mathbf{V}$ , respectively. Then,

$$(\mathbf{U} \circledast \mathbf{V})^H (\mathbf{H} \circledast \mathbf{F}) = (\mathbf{U}^H \mathbf{H}) \circledast (\mathbf{V}^H \mathbf{F}). \quad (4-37)$$

Now, let

$$\tilde{\boldsymbol{\beta}}_p = \text{vecb}(\tilde{\mathbf{B}}_p), \quad (4-38)$$

i.e.,

$$\tilde{\boldsymbol{\beta}}_p = \left[ \text{vec}^T(\mathbf{B}_{\hat{\theta}_1}) \cdots \text{vec}^T(\mathbf{B}_{\hat{\theta}_p}) \right]^T. \quad (4-39)$$

By using Lemma 1 (with  $K = 1$  and  $J = p$ ), we obtain:

$$\text{vec}(\tilde{\mathbf{Q}}_p^{-\frac{1}{2}} \tilde{\mathbf{A}}_p \tilde{\mathbf{B}}_p \tilde{\mathbf{S}}_p) = [\tilde{\mathbf{S}}_p^T \circledast (\tilde{\mathbf{Q}}_p^{-\frac{1}{2}} \tilde{\mathbf{A}})] \tilde{\boldsymbol{\beta}}_p \triangleq \tilde{\Gamma}_p \tilde{\boldsymbol{\beta}}_p. \quad (4-40)$$

Hence,

$$\begin{aligned} & \| \text{vec}(\tilde{\mathbf{Q}}_p^{-\frac{1}{2}} \mathbf{X} \Pi_{\tilde{\mathbf{S}}_p}) - \text{vec}(\tilde{\mathbf{Q}}_p^{-\frac{1}{2}} \tilde{\mathbf{A}}_p \tilde{\mathbf{B}}_p \tilde{\mathbf{S}}_p) \|^2 \\ &= \| \text{vec}(\tilde{\mathbf{Q}}_p^{-\frac{1}{2}} \mathbf{X} \Pi_{\tilde{\mathbf{S}}_p}) - \tilde{\Gamma}_p \tilde{\boldsymbol{\beta}}_p \|^2 \\ &\geq \| \text{vec}(\tilde{\mathbf{Q}}_p^{-\frac{1}{2}} \mathbf{X} \Pi_{\tilde{\mathbf{S}}_p}) \|^2 - \text{vec}^H(\tilde{\mathbf{Q}}_p^{-\frac{1}{2}} \mathbf{X} \Pi_{\tilde{\mathbf{S}}_p}) \tilde{\Gamma}_p (\tilde{\Gamma}_p^H \tilde{\Gamma}_p)^{-1} \tilde{\Gamma}_p^H \text{vec}(\tilde{\mathbf{Q}}_p^{-\frac{1}{2}} \mathbf{X} \Pi_{\tilde{\mathbf{S}}_p}) \\ &= L \text{tr}(\tilde{\mathbf{Q}}_p^{-1} \hat{\mathbf{R}}) - LM - \text{vecb}^H(\tilde{\mathbf{A}}_p^H \tilde{\mathbf{Q}}_p^{-1} \mathbf{X} \tilde{\mathbf{S}}_p^H) \times \\ &\quad \left[ (\tilde{\mathbf{S}}_p \tilde{\mathbf{S}}_p^H)^T \circledast (\tilde{\mathbf{A}}_p^H \tilde{\mathbf{Q}}_p^{-1} \tilde{\mathbf{A}}_p) \right]^{-1} \text{vecb}(\tilde{\mathbf{A}}_p^H \tilde{\mathbf{Q}}_p^{-1} \mathbf{X} \tilde{\mathbf{S}}_p^H), \end{aligned} \quad (4-41)$$

where we have used Lemmas 1 and 2, and the equality holds when

$$\tilde{\boldsymbol{\beta}} = (\tilde{\Gamma}_p^H \tilde{\Gamma}_p)^{-1} \tilde{\Gamma}_p^H \text{vec}(\tilde{\mathbf{Q}}_p^{-\frac{1}{2}} \mathbf{X} \Pi_{\tilde{\mathbf{S}}_p}). \quad (4-42)$$

By using (4-23), (4-25), (4-32) and (4-41), it follows that

$$\left[ \max_{\mathbf{Q}, \tilde{\mathbf{B}}_p} f(\mathbf{X} | \mathbf{H}_p) \right]^{\frac{1}{L}} \approx \frac{1}{(\pi e)^M g(\hat{\theta}_1, \dots, \hat{\theta}_p) |\tilde{\mathbf{Q}}_p|}, \quad (4-43)$$

where

$$g(\hat{\theta}_1, \dots, \hat{\theta}_p) = 1 - M + \text{tr}(\tilde{\mathbf{Q}}_p^{-1} \hat{\mathbf{R}}) - \frac{1}{L} \text{vecb}^H(\tilde{\mathbf{A}}_p^H \mathbf{Q}_p^{-1} \mathbf{X} \tilde{\mathbf{S}}_p^H) \times \\ \left[ (\tilde{\mathbf{S}}_p \tilde{\mathbf{S}}_p^H)^T \circledast (\tilde{\mathbf{A}}_p^H \mathbf{Q}_p^{-1} \tilde{\mathbf{A}}_p) \right]^{-1} \text{vecb}(\tilde{\mathbf{A}}_p^H \mathbf{Q}_p^{-1} \mathbf{X} \tilde{\mathbf{S}}_p^H). \quad (4-44)$$

Similarly, we have:

$$\left[ \max_{\mathbf{Q}, \tilde{\mathbf{B}}_{p+1}} f(\mathbf{X} | \mathbf{H}_{p+1}) \right]^{\frac{1}{L}} \approx \frac{1}{(\pi e)^M g(\theta, \hat{\theta}_1, \dots, \hat{\theta}_p) |\tilde{\mathbf{Q}}_{p+1}|}. \quad (4-45)$$

where  $\tilde{\mathbf{Q}}_{p+1}$  and  $g(\theta, \hat{\theta}_1, \dots, \hat{\theta}_p)$  are defined similarly to  $\tilde{\mathbf{Q}}_p$  in (4-27) and  $g(\hat{\theta}_1, \dots, \hat{\theta}_p)$  in (4-44), respectively.

Substituting (4-43) and (4-45) into (4-22) yields the conditional GLR:

$$\rho(\theta | \{\hat{\theta}_j\}) = \left\{ 1 - \frac{g(\theta, \hat{\theta}_1, \dots, \hat{\theta}_p) |\tilde{\mathbf{Q}}_{p+1}|}{g(\hat{\theta}_1, \dots, \hat{\theta}_p) |\tilde{\mathbf{Q}}_p|} \right\}^L. \quad (4-46)$$

### 4.3 Iterative Generalized Likelihood Ratio Test (iGLRT)

The basic idea of the iterative generalized likelihood ratio test (iGLRT) is to detect and localize targets sequentially. In each step of the iteration, the results from the previous iterations and steps are exploited for the detection and localization of new targets by calculating cGLR. Specifically, we first perform GLRT to get the location of the dominant target, and the following targets are detected and localized by using cGLRT conditioned on the most recently available estimates. The detailed steps of iGLRT are described in Table I.

Once the locations of the targets are determined, the amplitudes of the reflected signals can be estimated by using the AML estimator in [24]:

$$\hat{\beta}_{\hat{K}} = [(\tilde{\mathbf{A}}_{\hat{K}}^H \tilde{\mathbf{Q}}_{\hat{K}}^{-1} \tilde{\mathbf{A}}_{\hat{K}}) \circledast (\tilde{\mathbf{S}}_{\hat{K}}^H \tilde{\mathbf{S}}_{\hat{K}})^T]^{-1} \text{vecb}(\tilde{\mathbf{A}}_{\hat{K}}^H \tilde{\mathbf{Q}}_{\hat{K}}^{-1} \mathbf{X} \tilde{\mathbf{S}}_{\hat{K}}^H), \quad (4-47)$$

where  $\tilde{\mathbf{A}}_{\hat{K}}$ ,  $\tilde{\mathbf{S}}_{\hat{K}}$  and  $\tilde{\mathbf{Q}}_{\hat{K}}$  are defined similar to  $\tilde{\mathbf{A}}_p$ ,  $\tilde{\mathbf{A}}_p$  and  $\tilde{\mathbf{Q}}_p$  in (4-18), (4-19) and (4-27), respectively.



Table 4-1: iGLRT algorithm

**Step I:**

- Calculate  $\rho(\theta)$  in (4-12) for each  $\theta$ .
- Compare  $\rho(\theta)$  to a threshold  $\rho_0$ : if  $\rho(\theta) < \rho_0$  for all  $\theta$ , then Stop; otherwise,  $\hat{\theta}_1 = \arg \max_{\theta} \rho(\theta)$ , go to Step II.

**Step II:** For  $k = 1, 2, \dots$ , do the following:

- Calculate  $\rho(\theta|\{\hat{\theta}_i\}_{i=1}^k)$  in (4-46) for each  $\theta$ .
- If  $\rho(\theta|\{\hat{\theta}_i\}_{i=1}^k) < \rho_0$  for all  $\theta$ , then go to Step III; otherwise,  $\hat{\theta}_{k+1} = \arg \max_{\theta} \rho(\theta|\{\hat{\theta}_i\}_{i=1}^k)$ .

**Step III:** Repeat the following substeps until convergence for  $k = 1, 2, \dots, K$  (suppose that  $\hat{K}$  targets are detected in Steps I and II)

- Calculate  $\rho(\theta|\{\hat{\theta}_i\}_{i \neq k})$  for each  $\theta$ .
- Update  $\hat{\theta}_k$  by  $\arg \max_{\theta} \rho(\theta|\{\hat{\theta}_i\}_{i \neq k})$ .

We note that Step III of the above iGLRT algorithm actually minimizes the function  $g(\theta_1, \dots, \theta_{\hat{K}})$  with respect to  $\{\theta_k\}_{k=1}^{\hat{K}}$  by using the cyclic minimization (CM) technique [33]. Under a mild condition, i.e.,  $L \gg \tilde{N}\hat{K}$ , we have  $g(\theta_1, \dots, \theta_{\hat{K}}) \geq 0$ . Furthermore, we know that the CM algorithm monotonically decreases the cost function. Hence, the iGLRT algorithm is convergent. When  $\hat{K}$  is the true number of targets, iGLRT reduces to an approximate (parametric) maximum likelihood estimator. As we will show via numerical examples, the mean-squared-error (MSE) of the estimate of iGLRT approaches the corresponding Cramér-Rao bound (CRB) for a large number of data samples. On the other hand, we note that iGLRT needs only one-dimensional search and hence is computationally efficient.

## CHAPTER 5

### NUMERICAL EXAMPLES

In this chapter, we first compare the Cramér-Rao bounds (CRBs) for MIMO radars with different antenna configurations, and then present the detection and localization performance of the proposed methods.

#### 5.1 Cramér-Rao bound

We first study the Cramér-Rao bound under various antenna configurations. Consider a MIMO radar system with  $M = N = 8$  antennas for transmitting and receiving. We assume that the receiving and transmitting antennas are grouped into multiple subarrays (each being a uniform linear array with half-wavelength spacing between adjacent elements):

- MIMO Radar A: 1 subarray with 8 antennas for transmitting and receiving;
- MIMO Radar B: 2 subarrays each with 4 antennas for transmitting, and 1 subarray with 8 antennas for receiving;
- MIMO Radar C: 8 subarrays each with 1 antenna for transmitting, and 1 subarray with 8 antennas for receiving;
- MIMO Radar D: 2 subarrays each with 4 antennas for transmitting and receiving.

We assume that the transmitted waveforms are linearly orthogonal to each other and the total transmitted power is fixed to be 1, i.e.,  $\mathbf{R}_{\Phi\Phi} = \frac{1}{N}\mathbf{I}$ .

We consider a scenario in which  $K = 3$  targets are located at  $\theta_1 = -40^\circ$ ,  $\theta_2 = -4^\circ$  and  $\theta_3 = 0^\circ$ , and the elements of  $\{\mathbf{B}_{\theta_k}\}_{k=1}^3$  are independently and identically distributed (i.i.d.) circularly symmetric complex Gaussian random variables with zero mean and unit variance. There is a strong jammer at  $10^\circ$  with amplitude 100, i.e., 40 dB above the reflected signals. The received signal has  $L = 128$  snapshots

and is corrupted by a zero-mean spatially colored Gaussian noise with an unknown covariance matrix. The  $(p, q)$ th element of the unknown noise covariance matrix is  $\frac{1}{\text{SNR}} 0.90^{|p-q|} e^{j\frac{(p-q)\pi}{2}}$ .

Figures 5-1(a) and 5-1(b) show the cumulative density functions (CDFs) of the CRBs for MIMO radar with various antenna configurations when  $\text{SNR}=20$  dB. (The CRB of  $\theta_2$  is similar to that of  $\theta_3$  and hence is not shown.) The CDFs are obtained by 2000 Monte-Carlo trials. In each trial, we generate the elements of  $\{\mathbf{B}_{\theta_k}\}_{k=1}^3$  randomly, and then calculate the corresponding CRBs using (A-18) given by in the Appendix. For comparison purposes, we also provide the CDF of the phased-array (single-input multiple-output) counterpart, i.e., the special case of the above MIMO radar when  $N = 1$ , with the same total transmission power. As expected, the MIMO radar provides much better performance than the phased-array counterpart. Due to the fading effect of the elements of  $\{\mathbf{B}_{\theta_k}\}_{k=1}^3$ , the CRB of MIMO Radar A varies within a large range. Within a 95% confidence interval (i.e., when CDF varies from 2.5% to 97.5%), its CRB for  $\theta_1$  varies approximately from  $5 \times 10^{-7}$  to  $5 \times 10^{-5}$ . The CRBs for MIMO Radar C varies within a small range.

To evaluate the CRB performance, we define an outage CRB [1] for a given probability  $p$ , denoted by  $\text{CRB}_p$ , as:

$$P(\text{CRB} \geq \text{CRB}_p) = p. \quad (5-1)$$

Figures 5-2(a) - (d) show the outage  $\text{CRB}_{0.01}$  and  $\text{CRB}_{0.1}$  of  $\theta_1$  and  $\theta_3$ , as functions of SNR. As expected, the SNR gains depend on the probability  $p$ . As we can see, when  $p = 0.01$ , MIMO Radar C outperforms the other radar configurations, and provides around 20 dB and 12 dB improvements in SNR compared to the phased-array and MIMO Radar A, respectively. On the other hand, Figure 5-2(d) shows that MIMO radars A and B outperform others when  $p = 0.1$ .



## 5.2 Target Detection and Localization

We focus below on MIMO Radar B, i.e., a MIMO radar system with 2 subarrays (each with 4 antennas) for transmitting and 1 subarray (with 8 antennas) for receiving.

We first consider a scenario in which 3 targets are located at  $\theta_1 = -40^\circ$ ,  $\theta_2 = -20^\circ$  and  $\theta_3 = 0^\circ$  with the corresponding elements in  $\mathbf{B}_{\theta_1}$ ,  $\mathbf{B}_{\theta_2}$  and  $\mathbf{B}_{\theta_3}$  being fixed to 2, 2 and 1, respectively. The other simulation parameters are the same as for Figure 5-1. The Frobenius norm of the spatial spectral estimates of  $\mathbf{B}_\theta$  versus  $\theta$ , obtained by using LS, Capon and APES are given by Figures 5-3(a)-(c). For comparison purposes, we show the true spatial spectrum via dashed lines in these figures. As seen from Figure 5-3, the LS method suffers from high-sidelobes and poor resolution problems. Due to the presence of the strong jamming signal, the LS estimator fails to work properly. Capon and APES possess excellent interference and jamming suppression capabilities. The Capon method gives very narrow peaks around the target locations. However, the Capon estimates of  $\mathbf{B}_{\theta_1}$ ,  $\mathbf{B}_{\theta_2}$  and  $\mathbf{B}_{\theta_3}$  are biased downward. The APES method gives more accurate estimates around the target locations but its resolution is worse than that of Capon. Note that in Figures 5-3(a)-(c), a false peak occurs at  $\theta = 10^\circ$  due to the presence of the strong jammer. Although the jammer waveform is statistically independent of the waveforms transmitted by the MIMO radar, a false peak still exists since the jammer is 40 dB stronger than the weakest target and the number of data samples is finite. Figures 5-3(d)-(e) give the GLRT, and the iGLRT results, as functions of the target location parameter  $\theta$ . For convenience, in Figure 5-3(e), we have included all cGLR functions obtained by iGLRT, each indicating one target. As expected, we get high GLRs (cGLRs) at the target locations and low GLRs (cGLRs) at other locations including the jammer location. By comparing the GLR with a threshold, the false peak due to the strong jammer can be detected and

rejected, and a correct estimate of the number of the targets can be obtained by both methods.

Next we consider a more challenging example, where  $\theta_2$  is  $-4^\circ$  while all the other simulation parameters are the same as before. As shown in Figure 5-4(c), the APES, Capon and GLRT methods fail to resolve the two closely spaced targets at  $\theta_2 = -4^\circ$  and  $\theta_3 = 0^\circ$ . On the other hand, iGLRT gives well-resolved peaks around the true target locations. To illustrate the procedure of the iGLRT algorithm, we give the GLR, and cGLRs obtained in Steps I and II of iGLRT in Figures 5-5(a)-(d). Figures 5-5(a)-(b) show the GLR  $\rho(\theta)$  and the cGLR  $\rho(\theta|\hat{\theta}_1)$ , respectively, where  $\hat{\theta}_1$  is the estimated location of target 1 from  $\rho(\theta)$ . As we can see, there is no peak at around  $\theta_3 = 0^\circ$  in both figures. Yet a clear peak is shown in  $\rho(\theta|\hat{\theta}_1, \hat{\theta}_2)$  in Figure 5-5(c), which indicates the existence and location of target 3. The cGLR  $\rho(\theta|\hat{\theta}_1, \hat{\theta}_2, \hat{\theta}_3)$  in Figure 5-5(d) shows that no additional target exists other than the targets at  $\hat{\theta}_1$ ,  $\hat{\theta}_2$  and  $\hat{\theta}_3$ . In other words, the iGLRT method correctly estimates the number of targets to be 3.

Now we consider the elements in  $\mathbf{B}_{\theta_1}$ ,  $\mathbf{B}_{\theta_2}$  and  $\mathbf{B}_{\theta_3}$  as i.i.d complex Gaussian random variables with mean zero and unit variance. The other parameters are the same as those in Figure 5-6. The Figures 5-6(a)-(b) present the CDFs of the MSEs of  $\theta_1$  and  $\theta_3$  as well as the CRBs, when  $\text{SNR} = 20$  dB and  $L = 128$ . As we can see, the MSEs of the iGLRT are very close to the corresponding CRBs. Figures 5-7(a)-(b) show the outage  $\text{MSE}_{0.1}$  and  $\text{CRB}_{0.1}$  when  $p = 0.1$  as functions of SNR when  $L = 128$ . Again, the MSEs are very close to the corresponding the CRBs, and decreases almost linearly as SNR increases. Figure 5-8 gives the outage  $\text{MSE}_{0.1}$  and  $\text{CRB}_{0.1}$  as functions of  $L$  when  $\text{SNR}=20$  dB. As expected, the outage  $\text{MSE}_{0.1}$  approaches the corresponding  $\text{CRB}_{0.1}$  as  $L$  increases.



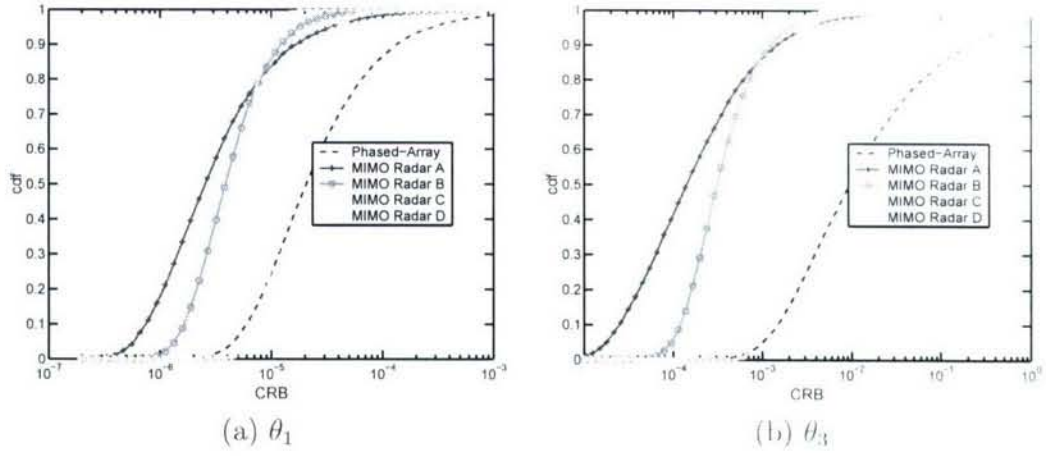


Figure 5-1: Cumulative density functions of the Cramér-Rao bounds for (a)  $\theta_1$  and (b)  $\theta_3$ .

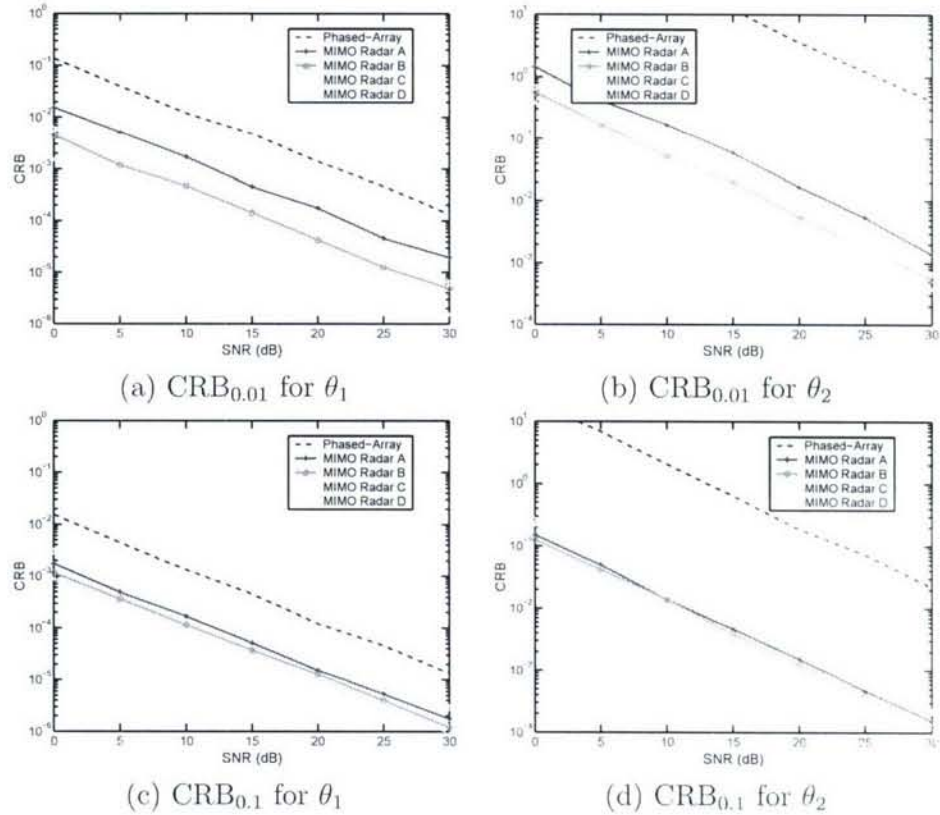


Figure 5-2: Outage CRB versus SNR. (a)  $\text{CRB}_{0.01}$  for  $\theta_1$ , (b)  $\text{CRB}_{0.01}$  for  $\theta_2$ , (c)  $\text{CRB}_{0.1}$  for  $\theta_1$ , and (d)  $\text{CRB}_{0.1}$  for  $\theta_2$ .

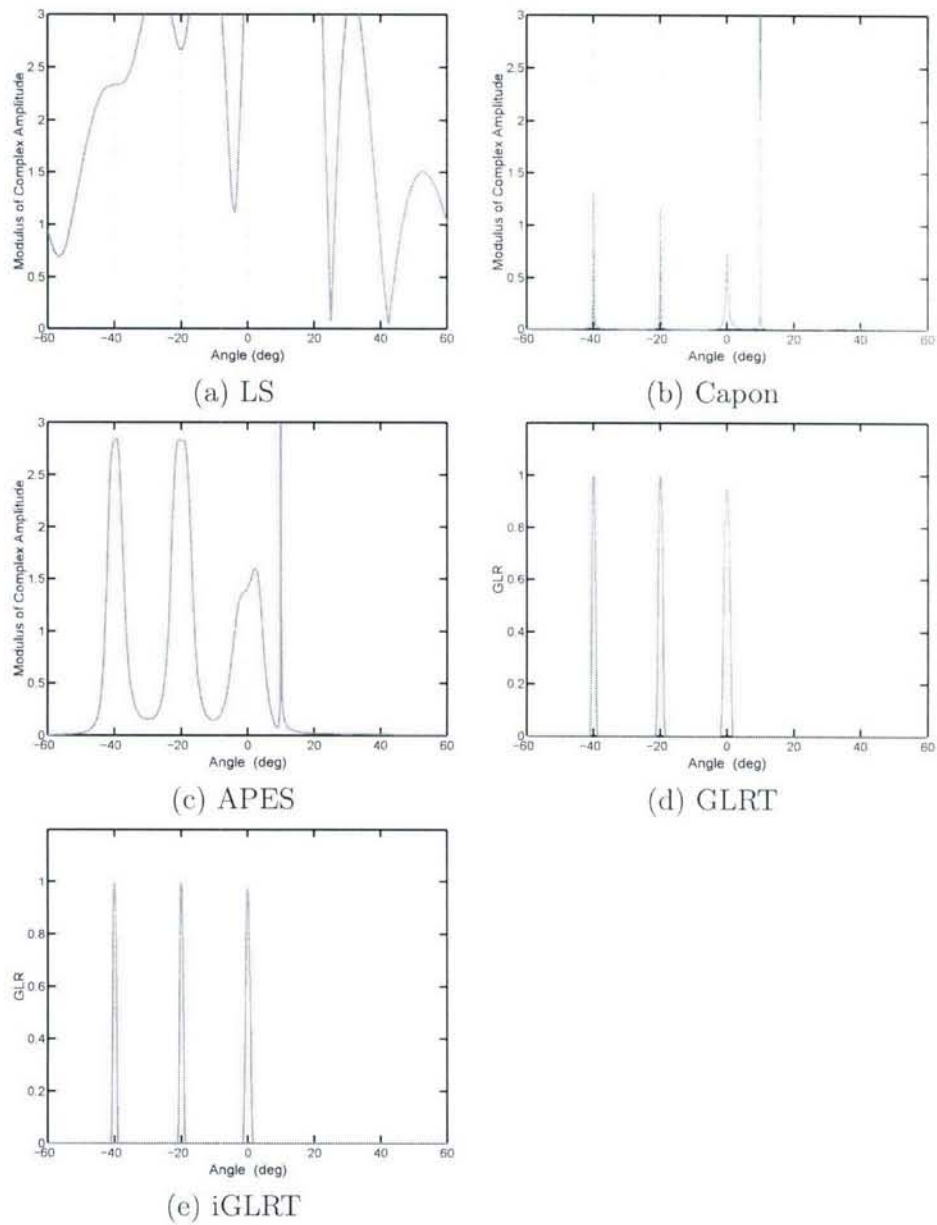


Figure 5-3: Spatial spectra, and GLR and cGLR Pseudo-Spectra when  $\theta_1 = 10^\circ$ ,  $\theta_2 = -20^\circ$ , and  $\theta_3 = 0^\circ$ . (a) LS, (b) Capon, (c) APES, (d) GLRT, and (e) iGLRT.

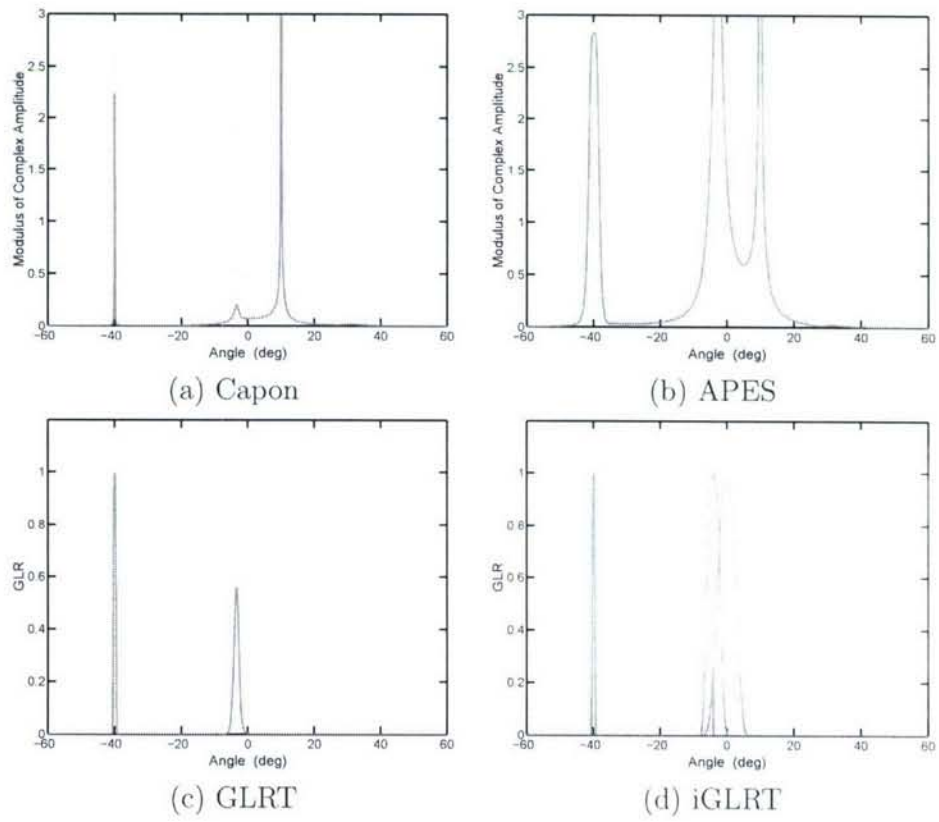


Figure 5-4: Spatial spectra, and GLR and cGLR Pseudo-Spectra, when  $\theta_1 = 10^\circ$ ,  $\theta_2 = -4^\circ$ , and  $\theta_3 = 0^\circ$ . (a) Capon, (b) APES, (c) GLRT, and (d) iGLRT.

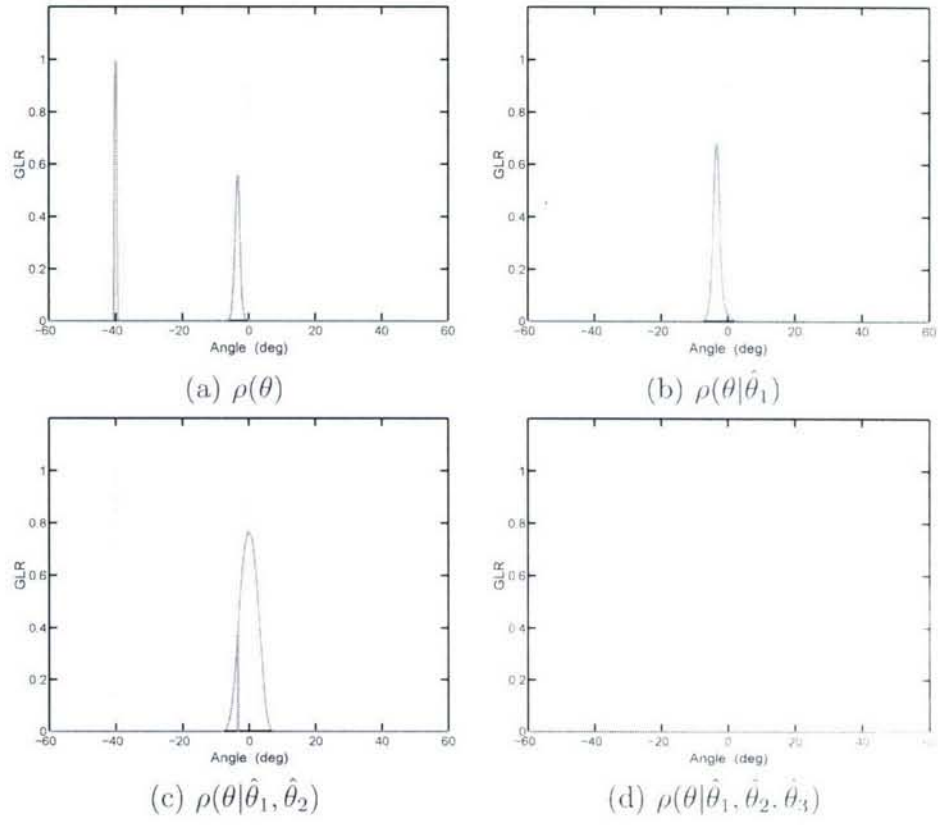


Figure 5-5: GLR and cGLR Pseudo-Spectra obtained in Steps I and II of iGLRT, when  $\theta_1 = -40^\circ$ ,  $\theta_2 = -4^\circ$ , and  $\theta_3 = 0^\circ$ . (a)  $\rho(\theta)$ , (b)  $\rho(\theta|\hat{\theta}_1)$ , (c)  $\rho(\theta|\hat{\theta}_1, \hat{\theta}_2)$ , and (d)  $\rho(\theta|\hat{\theta}_1, \hat{\theta}_2, \hat{\theta}_3)$ .

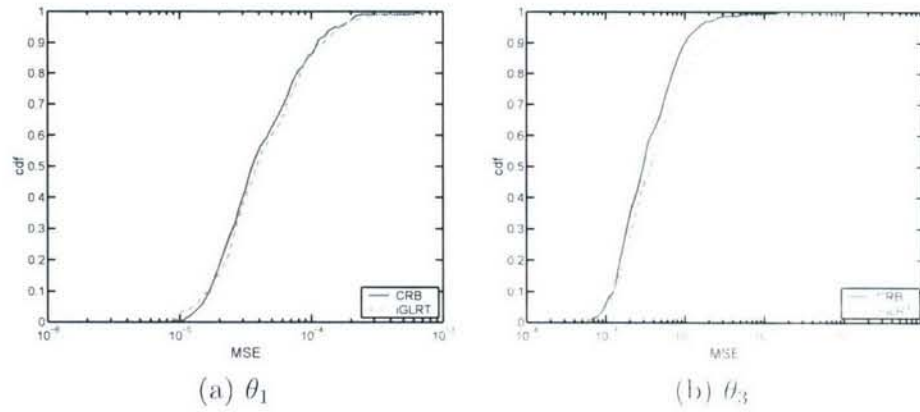


Figure 5-6: Cumulative density functions of the CRBs and MSEs for (a)  $\theta_1$  and (b)  $\theta_3$ .

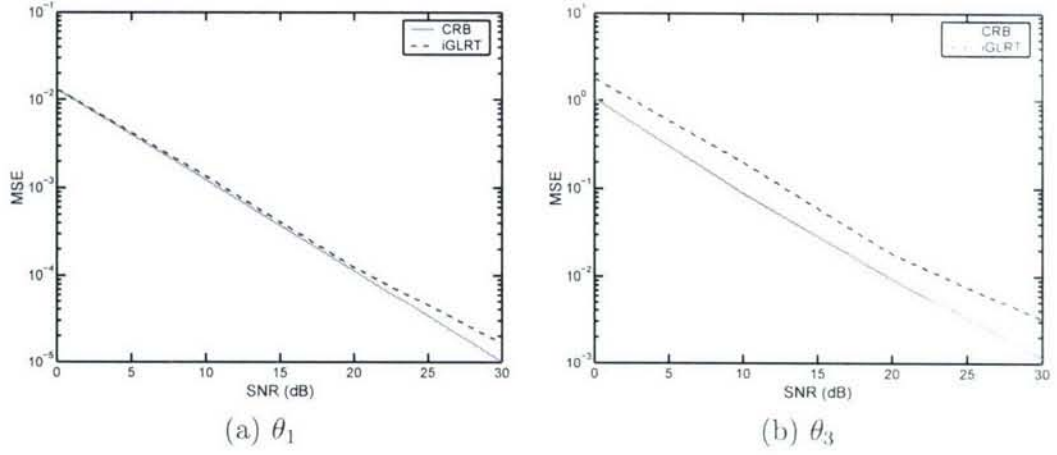


Figure 5-7: Outage  $\text{CRB}_{0.1}$  and  $\text{MSE}_{0.1}$  versus SNR for (a)  $\theta_1$  and (b)  $\theta_3$ .

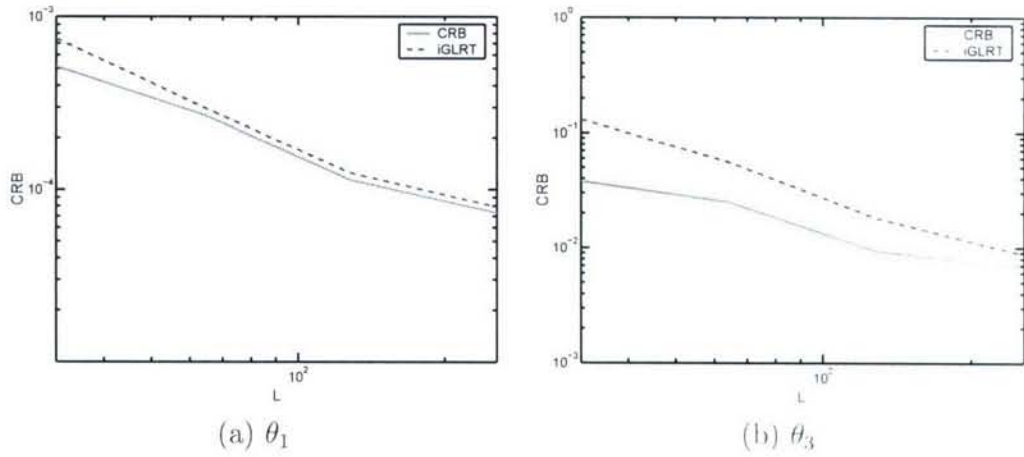


Figure 5-8: Outage  $\text{CRB}_{0.1}$  and  $\text{MSE}_{0.1}$  versus number of data samples for (a)  $\theta_1$  and (b)  $\theta_3$ .



## CHAPTER 6 CONCLUSIONS

We have considered a multiple-input multiple-output (MIMO) radar system with a general antenna configuration that can be used to achieve both the coherent processing gain and the spatial diversity gain. We have first introduced several spatial spectral estimators, including Capon and APES, for target detection and parameter estimation. By using our results on the growth curve models, we have provided a generalized likelihood ratio test (GLRT) and a conditional generalized likelihood ratio test (cGLRT), and then proposed an iterative GLRT (iGLRT) procedure for the MIMO radar system. Via several numerical examples, we have shown that the iGLRT method can provide excellent target detection and parameter estimation performance at a low computational cost.

## APPENDIX A CRAMÉR-RAO BOUND

Consider a MIMO radar system with  $K$  targets. Then the received signal can be written as

$$\mathbf{X} = \sum_{k=1}^K \mathbf{A}(\theta_k) \mathbf{B}_{\theta_k} \mathbf{V}^T(\theta_k) \Phi + \mathbf{Z}. \quad (\text{A-1})$$

Let

$$\boldsymbol{\theta} = [\theta_1 \ \cdots \ \theta_K]^T, \quad (\text{A-2})$$

$$\boldsymbol{\beta} = [\text{vec}^T(\mathbf{B}_{\theta_1}) \ \cdots \ \text{vec}^T(\mathbf{B}_{\theta_K})]^T, \quad (\text{A-3})$$

and

$$\boldsymbol{\beta}_R = \text{Re}(\boldsymbol{\beta}) \quad \boldsymbol{\beta}_I = \text{Im}(\boldsymbol{\beta}), \quad (\text{A-4})$$

where  $\text{Re}(\cdot)$  and  $\text{Im}(\cdot)$  denote the real and imaginary parts, respectively. Assume that the columns of  $\mathbf{Z}$  are *i.i.d.* circularly symmetric complex Gaussian random vectors with zero-mean and an unknown covariance matrix  $\mathbf{Q}$ .

Using the same argument as in Appendix A of [22], we know that the unknowns in  $\mathbf{Q}$  will not affect the CRBs of  $\boldsymbol{\beta}$  and  $\boldsymbol{\theta}$ . Hence, we need only to calculate the following Fisher information matrix with respect to  $\boldsymbol{\theta}$ ,  $\boldsymbol{\beta}_R$  and  $\boldsymbol{\beta}_I$ :

$$\text{FIM} = \begin{bmatrix} \mathbf{F}(\boldsymbol{\theta}, \boldsymbol{\theta}) & \mathbf{F}(\boldsymbol{\theta}, \boldsymbol{\beta}_R) & \mathbf{F}(\boldsymbol{\theta}, \boldsymbol{\beta}_I) \\ \mathbf{F}(\boldsymbol{\beta}_R, \boldsymbol{\theta}) & \mathbf{F}(\boldsymbol{\beta}_R, \boldsymbol{\beta}_R) & \mathbf{F}(\boldsymbol{\beta}_R, \boldsymbol{\beta}_I) \\ \mathbf{F}(\boldsymbol{\beta}_I, \boldsymbol{\theta}) & \mathbf{F}(\boldsymbol{\beta}_I, \boldsymbol{\beta}_R) & \mathbf{F}(\boldsymbol{\beta}_I, \boldsymbol{\beta}_I) \end{bmatrix}, \quad (\text{A-5})$$

where  $\mathbf{F}(\boldsymbol{\alpha}, \boldsymbol{\beta})$  denotes the Fisher information matrix with respect to  $\boldsymbol{\alpha}$  and  $\boldsymbol{\beta}$ .

Note that

$$F(\theta_i, \theta_j) = 2 \operatorname{Re} \operatorname{tr} \left\{ \frac{\partial \left[ \sum_{k=1}^K \mathbf{A}(\theta_k) \mathbf{B}_{\theta_k} \mathbf{V}^T(\theta_k) \Phi \right]^H}{\partial \theta_i} \times \mathbf{Q}^{-1} \frac{\partial \left[ \sum_{k=1}^K \mathbf{A}(\theta_k) \mathbf{B}_{\theta_k} \mathbf{V}^T(\theta_k) \Phi \right]}{\partial \theta_j} \right\}, \quad (\text{A } 6)$$

and

$$\frac{\partial \left[ \sum_{k=1}^K \mathbf{A}(\theta_k) \mathbf{B}_{\theta_k} \mathbf{V}^T(\theta_k) \Phi \right]}{\partial \theta_i} = \dot{\mathbf{A}}(\theta_i) \mathbf{B}_{\theta_i} \mathbf{V}^T(\theta_i) \Phi + \mathbf{A}(\theta_i) \mathbf{B}_{\theta_i} \dot{\mathbf{V}}^T(\theta_i) \Phi, \quad (\text{A } 7)$$

where

$$\dot{\mathbf{A}}(\theta_k) = \frac{\partial \mathbf{A}(\theta_k)}{\partial \theta} \quad \text{and} \quad \dot{\mathbf{V}}(\theta_k) = \frac{\partial \mathbf{V}(\theta_k)}{\partial \theta}. \quad (\text{A } 8)$$

Inserting (A-7) into (A-6) and after some matrix manipulations, we obtain:

$$\begin{aligned} F(\theta_i, \theta_j) = & 2L \operatorname{Re} \operatorname{tr} \left\{ [\dot{\mathbf{A}}^H(\theta_i) \mathbf{Q}^{-1} \dot{\mathbf{A}}(\theta_j)] [\mathbf{B}_{\theta_j} \mathbf{V}^T(\theta_j) \mathbf{R}_{\Phi\Phi} \mathbf{V}^*(\theta_i) \mathbf{B}_{\theta_i}^H] \right\} + \\ & 2L \operatorname{Re} \operatorname{tr} \left\{ [\dot{\mathbf{A}}^H(\theta_i) \mathbf{Q}^{-1} \mathbf{A}(\theta_j)] [\mathbf{B}_{\theta_j} \dot{\mathbf{V}}^T(\theta_j) \mathbf{R}_{\Phi\Phi} \mathbf{V}^*(\theta_i) \mathbf{B}_{\theta_i}^H] \right\} + \\ & 2L \operatorname{Re} \operatorname{tr} \left\{ [\mathbf{A}^H(\theta_i) \mathbf{Q}^{-1} \dot{\mathbf{A}}(\theta_j)] [\mathbf{B}_{\theta_j} \mathbf{V}^T(\theta_j) \mathbf{R}_{\Phi\Phi} \dot{\mathbf{V}}^*(\theta_i) \mathbf{B}_{\theta_i}^H] \right\} + \\ & 2L \operatorname{Re} \operatorname{tr} \left\{ [\mathbf{A}^H(\theta_i) \mathbf{Q}^{-1} \mathbf{A}(\theta_j)] [\mathbf{B}_{\theta_j} \dot{\mathbf{V}}^T(\theta_j) \mathbf{R}_{\Phi\Phi} \dot{\mathbf{V}}^*(\theta_i) \mathbf{B}_{\theta_i}^H] \right\}, \end{aligned} \quad (\text{A } 9)$$

where  $\mathbf{R}_{\Phi\Phi} = \frac{1}{L} \Phi \Phi^H$  is the covariance matrix of the transmitted waveforms. Hence,

$$\mathbf{F}(\boldsymbol{\theta}, \boldsymbol{\theta}) = 2 \operatorname{Re}(\mathbf{F}_{\theta\theta}), \quad (\text{A } 10)$$

where  $\mathbf{F}_{\theta\theta}$  is a  $K \times K$  matrix with its  $(i, j)$  element being:

$$\begin{aligned} [\mathbf{F}_{\theta\theta}]_{ij} = & L \operatorname{tr} \left\{ [\dot{\mathbf{A}}(\theta_i)^H \mathbf{Q}^{-1} \dot{\mathbf{A}}(\theta_j)] [\mathbf{B}_{\theta_j} \mathbf{V}^T(\theta_j) \mathbf{R}_{\Phi\Phi} \mathbf{V}^*(\theta_i) \mathbf{B}_{\theta_i}^H] \right\} + \\ & L \operatorname{tr} \left\{ [\dot{\mathbf{A}}^H(\theta_i) \mathbf{Q}^{-1} \mathbf{A}(\theta_j)] [\mathbf{B}_{\theta_j} \dot{\mathbf{V}}^T(\theta_j) \mathbf{R}_{\Phi\Phi} \mathbf{V}^T(\theta_i) \mathbf{B}_{\theta_i}^H] \right\} + \\ & L \operatorname{tr} \left\{ [\mathbf{A}^H(\theta_i) \mathbf{Q}^{-1} \dot{\mathbf{A}}(\theta_j)] [\mathbf{B}_{\theta_j} \mathbf{V}^T(\theta_j) \mathbf{R}_{\Phi\Phi} \dot{\mathbf{V}}^*(\theta_i) \mathbf{B}_{\theta_i}^H] \right\} + \\ & L \operatorname{Re} \left\{ [\mathbf{A}^H(\theta_i) \mathbf{Q}^{-1} \mathbf{A}(\theta_j)] [\mathbf{B}_{\theta_j} \dot{\mathbf{V}}^T(\theta_j) \mathbf{R}_{\Phi\Phi} \dot{\mathbf{V}}^*(\theta_i) \mathbf{B}_{\theta_i}^H] \right\}. \end{aligned} \quad (\text{A } 11)$$

Similarly, we have

$$\mathbf{F}^T(\boldsymbol{\theta}, \boldsymbol{\beta}_R) = \mathbf{F}(\boldsymbol{\beta}_R, \boldsymbol{\theta}) = 2 \operatorname{Re}(\mathbf{F}_{\beta\theta}), \quad (\text{A-12})$$

$$\mathbf{F}^T(\boldsymbol{\theta}, \boldsymbol{\beta}_I) = \mathbf{F}(\boldsymbol{\beta}_I, \boldsymbol{\theta}) = 2 \operatorname{Im}(\mathbf{F}_{\beta\theta}), \quad (\text{A-13})$$

$$\mathbf{F}(\boldsymbol{\beta}_R, \boldsymbol{\beta}_R) = \mathbf{F}(\boldsymbol{\beta}_I, \boldsymbol{\beta}_I) = 2 \operatorname{Re}(\mathbf{F}_{\beta\beta}), \quad (\text{A-14})$$

and

$$\mathbf{F}^T(\boldsymbol{\beta}_R, \boldsymbol{\beta}_I) = \mathbf{F}(\boldsymbol{\beta}_I, \boldsymbol{\beta}_R) = 2 \operatorname{Im}(\mathbf{F}_{\beta\beta}), \quad (\text{A-15})$$

where  $\mathbf{F}_{\theta\beta}$  and  $\mathbf{F}_{\beta\beta}$  are both partitioned matrices with  $K \times K$  and  $K \times K$  blocks and with their submatrices being, respectively,

$$\begin{aligned} [\mathbf{F}_{\beta\theta}]_{ij} = & L \operatorname{vec} \left\{ [\mathbf{A}^H(\theta_i) \mathbf{Q}^{-1} \dot{\mathbf{A}}(\theta_j)] [\mathbf{B}_{\theta_j} \mathbf{V}^T(\theta_j) \mathbf{R}_{\Phi\Phi} \mathbf{V}^*(\theta_i)] \right\} + \\ & L \operatorname{vec} \left\{ [\mathbf{A}^H(\theta_i) \mathbf{Q}^{-1} \mathbf{A}(\theta_j)] [\mathbf{B}_{\theta_j} \dot{\mathbf{V}}^T(\theta_j) \mathbf{R}_{\Phi\Phi} \mathbf{V}^*(\theta_i)] \right\} \end{aligned} \quad (\text{A-16})$$

and

$$[\mathbf{F}_{\beta\beta}]_{ij} = L [\mathbf{V}^T(\theta_i) \mathbf{R}_{\Phi\Phi} \mathbf{V}^*(\theta_j)] \otimes [\mathbf{A}^H(\theta_i) \mathbf{Q}^{-1} \mathbf{A}(\theta_j)], \quad (\text{A-17})$$

with  $\otimes$  denoting the Kronecker product.

Substituting Equations (A-9) - (A-15) into (A-6), and after some matrix manipulations, we get

$$\operatorname{CRB}(\boldsymbol{\theta}) = \frac{1}{2} \left\{ \operatorname{Re} [\mathbf{F}_{\theta\theta} - \mathbf{F}_{\theta\beta} \mathbf{F}_{\beta\beta}^{-1} \mathbf{F}_{\theta\beta}^H] \right\}^{-1}, \quad (\text{A-18})$$

and

$$\operatorname{CRB}(\boldsymbol{\beta}) = \mathbf{F}_{\beta\beta}^{-1} + \mathbf{F}_{\beta\beta}^{-1} \mathbf{F}_{\theta\beta}^H \operatorname{CRB}(\boldsymbol{\theta}) \mathbf{F}_{\theta\beta} \mathbf{F}_{\beta\beta}^{-1}. \quad (\text{A-19})$$

## REFERENCES

- [1] E. Fishler, A. Haimovich, R. Blum, D. Chizhik, L. Cimini, and R. Valenzuela, "MIMO radar: an idea whose time has come," *Proceedings of the IEEE Radar Conference*, pp. 71–78, April 2004.
- [2] E. Fishler, A. Haimovich, R. Blum, L. Cimini, D. Chizhik, and R. Valenzuela, "Performance of MIMO radar systems: advantages of angular diversity," *38th Asilomar Conference on Signals, Systems and Computers*, Pacific Grove, CA, vol. 1, pp. 305–309, November 2004.
- [3] E. Fishler, A. Haimovich, R. Blum, L. Cimini, D. Chizhik, and R. Valenzuela, "Spatial diversity in radars - models and detection performance," *IEEE Transactions on Signal Processing*, vol. 54, pp. 823–838, March 2006.
- [4] N. Lehmann, E. Fishler, A. M. Haimovich, R. S. Blum, D. Chizhik, L. Cimini, and R. Valenzuela, "Evaluation of transmit diversity in MIMO-radar direction finding," Submitted to *IEEE Transactions on Signal Processing*, 2005.
- [5] D. R. Fuhrmann and G. San Antonio, "Transmit beamforming for MIMO radar systems using partial signal correlations," *38th Asilomar Conference on Signals, Systems and Computers*, Pacific Grove, CA, vol. 1, pp. 295–299, November 2004.
- [6] J. Li, P. Stoica, and Y. Xie, "On probing signal design for MIMO radar," *40th Asilomar Conference on Signals, Systems and Computers* (invited), Pacific Grove, CA, October 2006.
- [7] A. S. Fletcher and F. C. Robey, "Performance bounds for adaptive coherence of sparse array radar," *Proc. of the 11th Conf. on Adaptive Sensors Array Processing*, March 2003.
- [8] D. W. Bliss and K. W. Forsythe, "Multiple-input multiple-output (MIMO) radar and imaging: degrees of freedom and resolution," *37th Asilomar Conference on Signals, Systems and Computers*, Pacific Grove, CA, vol. 1, pp. 54–59, November 2003.
- [9] F. C. Robey, S. Coutts, D. Weikle, J. C. McHarg, and K. Cuomo, "MIMO radar theory and experimental results," *38th Asilomar Conference on Signals, Systems and Computers*, Pacific Grove, CA, vol. 1, pp. 300–304, November 2004.
- [10] K. Forsythe, D. Bliss, and G. Fawcett, "Multiple-input multiple-output (MIMO) radar: performance issues," *38th Asilomar Conference on Signals, Systems and Computers*, Pacific Grove, CA, vol. 1, pp. 310–315, November 2004.



- [11] L. B. White and P. S. Ray, "Signal design for MIMO diversity systems," *38th Asilomar Conference on Signals, Systems and Computers*, Pacific Grove, CA, vol. 1, pp. 973 – 977, November 2004.
- [12] I. Bekkerman and J. Tabrikian, "Spatially coded signal model for active arrays," *The 2004 IEEE International Conference on Acoustics, Speech, and Signal Processing*, Montreal, Quebec, Canada, vol. 2, pp. ii/209–ii/212, March 2004.
- [13] J. Tabrikian and I. Bekkerman, "Transmission diversity smoothing for multi-target localization," *The 2005 IEEE International Conference on Acoustics, Speech, and Signal Processing*, Philadelphia, PA, vol. 4, pp. iv/1041–iv/1044, March 2005.
- [14] J. Tabrikian, "Barankin bounds for target localization by MIMO radars," *4th IEEE Workshop on Sensor Array and Multi-channel Processing*, Waltham, MA, July 2006.
- [15] I. Bekkerman and J. Tabrikian, "Target detection and localization using MIMO radars and sonars,"
- [16] L. Xu, J. Li, and P. Stoica, "Adaptive techniques for MIMO radar," *4th IEEE Workshop on Sensor Array and Multi-channel Processing*, Waltham, MA, July 2006.
- [17] L. Xu, J. Li, and P. Stoica, "Radar imaging via adaptive MIMO techniques," *14th European Signal Processing Conference*, (invited), Florence, Italy, September 2006.
- [18] J. Li, P. Stoica, L. Xu, and W. Roberts, "On parameter identifiability of MIMO radar," *IEEE Signal Processing Letters*, to appear, available at [http://www.sal.ufl.edu/sal/MIMO\\_Identifiability.pdf](http://www.sal.ufl.edu/sal/MIMO_Identifiability.pdf).
- [19] M. I. Skolnik, *Introduction to Radar System*, 3rd ed. New York, NY: McGraw-Hill, 2002.
- [20] J. Capon, "High resolution frequency-wavenumber spectrum analysis," *Proceedings of the IEEE*, vol. 57, pp. 1408–1418, August 1969.
- [21] A. Dogandžić and A. Nehorai, "Generalized multivariate analysis of variance," *IEEE Signal Processing Magazine*, pp. 39–54, September 2003.
- [22] L. Xu and J. Li, "Performance analysis of multivariate complex amplitude estimators," *IEEE Transactions on Signal Processing*, vol. 53, pp. 3162–3171, August 2005.
- [23] L. Xu, P. Stoica, and J. Li, "A diagonal growth curve model and some signal processing applications," *IEEE Transactions on Signal Processing*, vol. 54, pp. 3363–3371, September 2006.

- [24] L. Xu, P. Stoica, and J. Li, "A block diagonal growth curve model," *Digital Signal Processing*, vol. 16, pp. 902–912, 2006.
- [25] J. Li and P. Stoica, "An adaptive filtering approach to spectral estimation and SAR imaging," *IEEE Transactions on Signal Processing*, vol. 44, pp. 1169–1181, June 1996.
- [26] P. Stoica and R. L. Moses, *Spectral Analysis of Signals*. Upper Saddle River, NJ: Prentice-Hall, 2005.
- [27] P. Stoica, H. Li, and J. Li, "Amplitude estimation for sinusoidal signals with application to system identification," *IEEE Transactions on Signal Processing*, vol. 48, pp. 338–352, February 2000.
- [28] H. Wang and L. Cai, "On adaptive multiband signal detection with GLR algorithm," *IEEE Transactions on Aerospace and Electronic Systems*, vol. 27, pp. 225–233, Mar. 1991.
- [29] E. J. Kelly, "Finite-sum expressions for signal detection probabilities," Technical Report 566, Lincoln Laboratory, M.I.T, May 1981.
- [30] D. A. Harville, *Matrix Algebra from a Statistician's Perspective*. New York, NY: Springer, Inc., 1997.
- [31] J. Li, B. Halder, P. Stoica, and M. Viberg, "Computationally efficient angle estimation for signals with known waveforms," *IEEE Transactions on Signal Processing*, vol. 43, pp. 2154–2163, September 1995.
- [32] S. Liu, "Matrix results on the Khatri-Rao and Tracy-Singh products," *Linear Algebra and its Applications*, vol. 289, pp. 267–277, 1999.
- [33] P. Stoica and Y. Selén, "Cyclic minimizers, majorization techniques, and expectation-maximization algorithm: A refresher," *IEEE Signal Processing Magazine*, pp. 112–114, January 2004.